Published August 11, 2008

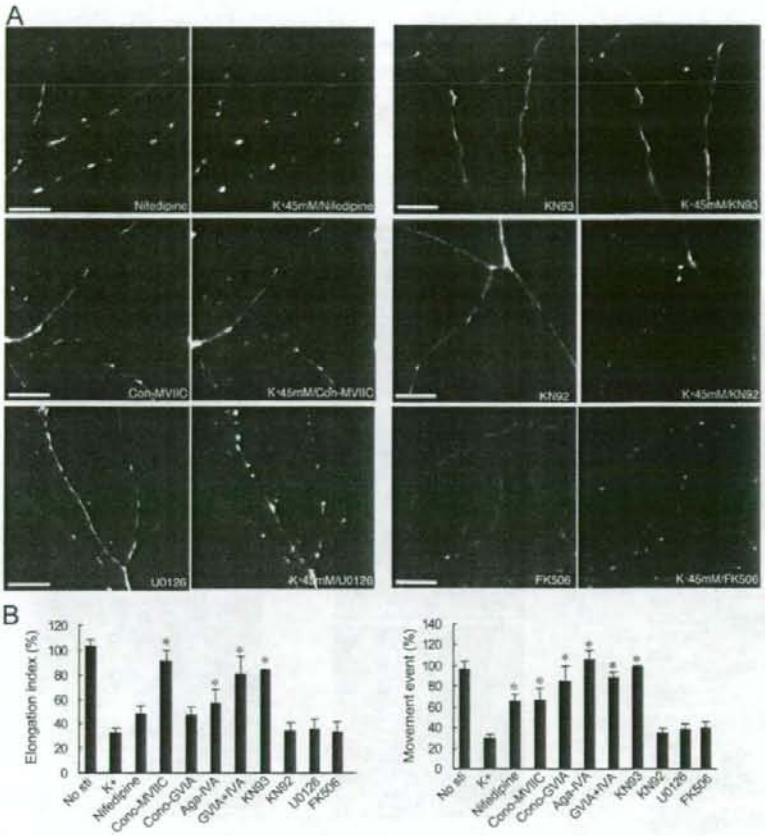

Figure 3. **VDCC-associated Ca^{2+} signaling is involved in the effects of high K^+ on mitochondria.** (A) Neurons (10 DIV) transfected with pDsRed2-Mito were analyzed by time-lapse imaging. Neurons (at 11 DIV) were then preincubated with 10 µM nifedipine (L-type blocker), 1 µM Cono-MVIIC (N and P/Q blocker), 10 µM UO126 (MAPK inhibitor), 20 µM KN93 (CaMK inhibitor), 20 µM KN92 (control for KN93), and 1 µM FK506 and were incubated in 45 mM K^+ for 15 min. Bars, 10 µm. (B) Mitochondrial length was measured through analysis of the elongation index (calculated by the square of longest length divided by the area). The elongation index after 15 min of high K^+ stimulation was normalized to the value before stimulation. Mitochondrial movement was measured by time-lapse fluorescence microscopy. The movement events after high K^+ stimulation were normalized to the value before stimulation. Neurons were either untreated (No sti), incubated with 45 mM K^+ for 15 min (K^+), or preincubated with various pharmacological agents before incubation with 45 mM K^+ as in A and also including 1 µM Cono-GVIA (N-type blocker), 0.1 µM Aga-IVA (P/Q-type blocker), or Cono-GVIA plus Aga-IVA. The results shown are from five experiments and represent the mean ± SEM ($n = 5$) in each group. Values were analyzed using one-way ANOVA followed by post-Tukey test. *, $P < 0.05$ versus K^+ stimulation.

neurons. Ca^{2+} signaling via VDCCs stimulates mitochondrial fragmentation, and this involves activation of Ca^{2+}/calmodulin-dependent protein kinase I (CaMKI) and phosphorylation of Drp1 at serine 600 (Ser600). These results identify an important mechanism involved in Drp1-regulated mitochondrial dynamics and highlight a key role for Ca^{2+} in the control of mitochondrial dynamics.

Results

Effects of high K^+ on mitochondrial dynamics and morphology in neurons

Cultured hippocampal neurons were transfected with pDsRed2-Mito to label mitochondria. The movement and morphology of mitochondria were monitored using live-cell imaging. As previously demonstrated (Ligon and Steward, 2000), mitochondria were found in neuronal axons and dendrites, exhibiting an elongated shape and dynamic movement. Treatment with 45 mM K^+ for 15 min had a marked effect on mitochondrial shape and movement. Elongated mitochondria became much shorter and rounder in morphology (Fig. 1 A and Fig. S1, A and C, available at http://www.jcb.org/cgi/content/full/jcb.200802164/DC1). In time-lapse imaging, 45-mM K^+ stimulation was found to trigger a rapid halt to movement (mitochondrial movement was reduced to 16.5% of control at 1 min, recovering to 26.3% at 10 min and 29.6% at 15 min; Fig. S1, A and B). High K^+ treatment also caused mitochondria to form ringlike structures that were the sites of fission events giving rise to smaller, round mitochondrial structures (Fig. 1 B).

Mitochondrial morphology was also assessed by electron microscopy. Normal mitochondria had a rodlike shape with clear cristae (Fig. 1 C, i and ii). After high K^+ treatment, mitochondria appeared empty with less electron-dense material and less cristae (Fig. 1 C, iii–vii). Mitochondria undergoing division were frequently observed. In some cases, the dividing mitochondria were found to be connected by a narrow necklike membrane (Fig. 1 C, v–vii).

VDCC-associated Ca^{2+} signaling is required for the effects of high K^+ on mitochondrial dynamics

To investigate the signaling mechanisms involved in the effects of high K^+ on mitochondria, we first measured intracellular Ca^{2+} level after high K^+ treatment. As expected, high K^+ stimulation triggered a rapid increase in intracellular Ca^{2+}. The increased Ca^{2+} was sustained during the 20-min treatment with high K^+ and then rapidly recovered to a normal level after washout of K^+ (Fig. 2 A). The changes in mitochondrial movement and morphology were observed in response to various concentrations of K^+ from 10 to 100 mM (not depicted) but, importantly, were

Published August 11, 2008

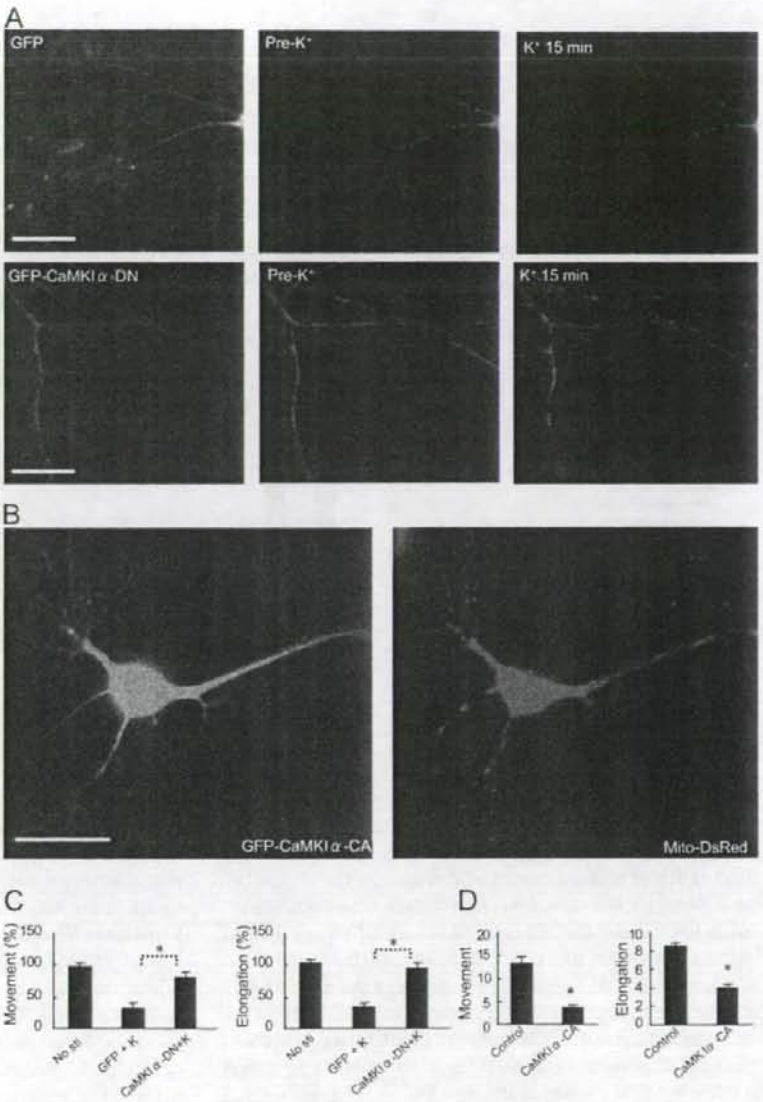

Figure 4. **CaMKIα mediates VDCC-dependent mitochondrial changes after high K+.** (A) Neurons (10 DIV) were cotransfected with pDsRed2-Mito and GFP (negative control; top) or GFP–CaMKIα-DN. Neurons (at 11 DIV) were treated with 45 mM K^+ for 15 min. GFP fluorescence is shown in the left panels, and mitochondrial fluorescence is shown before (Pre-K^+) and after high K^+ treatment in the middle and right panels. Bars, 20 µm. (B) Neurons were transfected with GFP–CaMKIα-CA and pDsRed2-Mito. GFP fluorescence is shown in the left panel, and mitochondrial fluorescence is shown in the right panel. Bar, 20 µm. (C) Mitochondrial movement or length was measured for neurons that were either untreated (no stimulation) or treated with 45 mM K^+ as shown in A. The movement events after high K^+ stimulation were normalized to the value obtained before stimulation. The elongation index after 15 min of high K^+ stimulation was also normalized to the value obtained before stimulation. Data were obtained from >150 mitochondria in three to five independent experiments for each condition. Error bars indicate SEM in each group. *, $P < 0.001$. (D) Mitochondrial movement or elongation index was measured for neurons that were either untreated (Control; transfected with GFP) or after transfection with GFP–CaMKI-CA as in B. Mitochondrial movement was measured by time-lapse fluorescence microscopy. Mitochondrial length was measured through analysis of the elongation index. Data were obtained from at least 350 mitochondria in 7–10 neurons for each condition. Error bars indicate SEM in each group. *, $P < 0.001$.

reversible after 15-min treatment with high K^+ and subsequent washout (Fig. 2 B). Furthermore, we found that there was little detectable neuronal death 24 h after high K^+ treatment (15 min) and subsequent washout (Fig. 2 C). In contrast, as expected, treatment with glutamate (500 µM for 15 min) resulted in obvious cell death when examined 24 h later.

To investigate the identity of Ca^{2+} channels involved in the regulation of mitochondrial dynamics, we examined the effects of a series of VDCC inhibitors (Fig. 3). All of the VDCC blockers (N, P/Q, and L type) attenuated the high K^+–induced changes in mitochondrial movement (Fig. 3 B). However, only the N-type VDCC blocker, P/Q-type VDCC blocker (conotoxin-MVIIC or a mix of conotoxin-GVIA and agatoxin-IVA), and P/Q-type blocker agatoxin IVA prevented high K^+–induced changes in mitochondrial morphology (Fig. 3, A and B). These results suggest that either L-, N-, or P/Q-type VDCC may be involved in K^+-induced mitochondrial dynamics but that coactivation of N and P/Q types plays the most important role.

CaMKIα mediates VDCC-dependent mitochondrial changes

We next investigated the role of intracellular Ca^{2+}-dependent signaling pathways that might be involved in control of mitochondrial dynamics. FK506 and cyclosporin, which act through inhibition of the Ca^{2+}-dependent protein phosphatase, calcineurin, had no effect on high K^+–induced changes in mitochondrial shape and movement (Fig. 3, A and B). U0126, a blocker of extracellular signal-regulated kinase signaling, also had no effect on K^+-induced changes (Fig. 3, A and B). However, KN93, an antagonist of CaMKs, almost completely blocked the K^+-induced

Published August 11, 2008

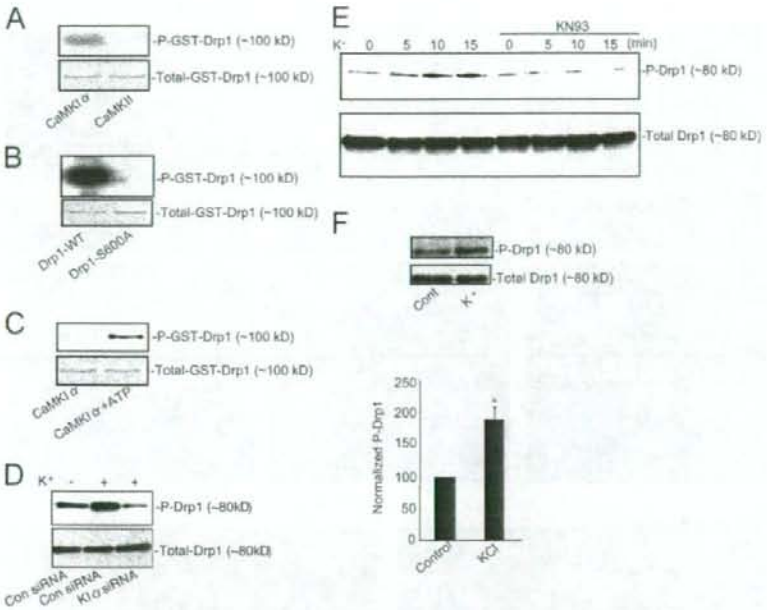

Figure 5. **CaMKIα phosphorylates recombinant Drp1 and endogenous Drp1 in cells.** (A) Recombinant Drp1 was incubated with either CaMKIα or CaMKII as indicated in the presence of [^{32}P]ATP. Proteins were separated by SDS-PAGE and analyzed by autoradiography and Coomassie staining. (B) Wild-type Drp1 or mutant Drp1 in which Ser600 was replaced by alanine was incubated with CaMKIα and [^{32}P]ATP, and proteins were separated by SDS-PAGE and analyzed by autoradiography. (C) Recombinant Drp1 was incubated with CaMKIα in the absence or presence of ATP. Proteins were separated by SDS-PAGE and analyzed by immunoblotting using a phospho-specific antibody selective for phospho-Ser600. (D) HeLa cells were transfected without (control siRNA) or with siRNA selective for CaMKIα. HeLa cells were incubated without (−) or with 45 mM K^+ for 15 min (+). Proteins were separated by SDS-PAGE and analyzed by immunoblotting with phospho-Ser600 or Drp1 antibodies. (E) Neurons were incubated for the indicated times with 45 mM K^+ in the absence or presence of KN93 (20 μM added 30 min before high K^+). Proteins were separated by SDS-PAGE and analyzed by immunoblotting with phospho-Ser600 or Drp1 antibodies as indicated. (F) Neurons were untreated (control) or treated with 45 mM K^+ for 15 min. Proteins were separated by SDS-PAGE and analyzed by immunoblotting with phospho-Ser600 or total Drp1 antibodies as indicated (bottom). Bar graphs show cumulative data from three independent experiments for each condition. Error bars indicate SEM in each group. *, $P < 0.05$.

changes in mitochondrial shape and movement (Fig. 3, A and B). KN92, a negative control for KN93, had no effect. The inhibitory effect of KN93 was not caused by an effect on Ca^{2+} influx because KN93 (or KN92) had no effect on high K^+–induced elevation in intracellular Ca^{2+} (unpublished data). KN93 is a general inhibitor of CaMKs, including CaMKI, CaMKII, and CaMKIV, but recent studies in neurons have highlighted that CaMKI may be an important target for KN93 (Schmitt et al., 2005). Therefore, we assessed the possible contribution of CaMKIα, the most abundant CaMKI isoform (Hook and Means, 2001), in the regulation of mitochondrial dynamics and morphology. Expression of a dominant-negative CaMKIα (CaMKIα-DN) blocked the effect of high K^+ on mitochondrial length and movement (Fig. 4, A and C). In addition, expression of constitutively active CaMKIα (CaMKIα-CA) alone resulted in inhibition of mitochondrial movement and caused mitochondria to become shorter in length (Fig. 4, B and D).

Ser600 of Drp1 is phosphorylated by CaMKIα

We next investigated whether proteins involved in mitochondrial fission might be phosphorylated by CaMKIα. Drp1 is an important protein involved in the scission of mitochondrial membranes (Frank et al., 2001; Smirnova et al., 2001; Yoon et al., 2003). Based on the consensus sequence of CaMKI (Lee et al., 1994; Matsushita and Nairn, 1998), there is a potential evolutionary conserved phosphorylation site at Ser600 in Drp1-3 (Drp1 isoform 3 as well as other isoforms; Fig. S2 A, available at http://www.jcb.org/cgi/content/full/jcb.200802164/DC1). In vitro assays indicated that recombinant Drp1 was phosphorylated by CaMKIα but was not phosphorylated by CaMKII (Fig. 5 A). Mutation of Ser600 (to alanine) resulted in a loss of phosphorylation by CaMKIα (Fig. 5 B). Phosphorylation of Ser600 was further confirmed by a phosphoantibody that specifically recognized phospho-Ser600 (Fig. 5 C). We then examined the phosphorylation of Drp1 by CaMKIα in intact cells. In HeLa cells, high K^+ treatment increased phosphorylation of Drp1 at Ser600, and the phosphorylation was prevented after down-regulation of CaMKIα levels using RNAi (control studies indicated that CaMKIα was down-regulated by >80% using human CaMKIα RNAi; Fig. 5 D and Fig. S2 B). In primary cultured neurons, high K^+ treatment also increased phosphorylation of Drp1 at Ser600, and this was prevented by preincubation with KN93 (Fig. 5, E and F). Together, these results strongly suggest that Drp1 is a physiological substrate for CaMKIα and that phosphorylation can be selectively stimulated through activation of VDCCs.

Drp1-S600 phosphorylation is required for the effects of high K^+ on mitochondrial dynamics

We next examined the functional consequences of Drp1 phosphorylation on mitochondrial morphology. These studies were performed both in HeLa cells and in cultured neurons. In HeLa

Published August 11, 2008

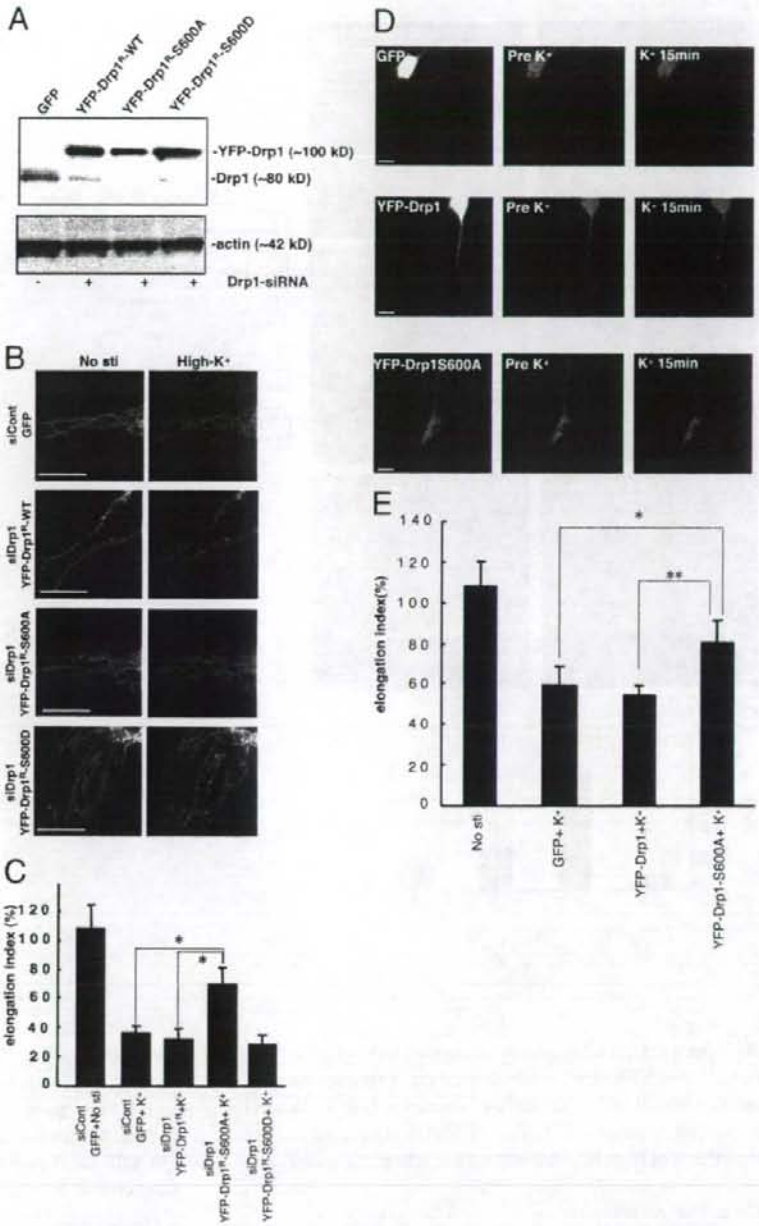

Figure 6. **Drp1-S600 phosphorylation is required for the effects of high K^+ on mitochondrial dynamics.** (A) HeLa cells were first transfected with control siRNA (siCont; Invitrogen) and siRNA for Drp1 (siDrp1) before transfection with the Drp1 plasmids. 1 d later, HeLa cells were transfected with GFP, YFP-Drp1^R, YFP-Drp1^R-S600A, or YFP-Drp1^R-S600D together with pDsRed2-Mito. Proteins were separated by SDS-PAGE and analyzed by immunoblotting using Drp1 and actin antibodies. (B) HeLa cells were treated without (No sti) or with 20 mM K^+ (high K^+), and mitochondrial fluorescence was analyzed by time-lapse imaging. Mitochondrial length was measured through analysis of the elongation index. Bars, 5 μm. (C) The elongation index was normalized to the value before stimulation. Values shown are the mean ± SEM ($n = 5$) in each group. Values were analyzed using one-way ANOVA followed by post-Tukey test. *, $P < 0.01$. (D) Neurons (10 DIV) were cotransfected with pDsRed2-Mito and GFP, YFP-Drp1, or YFP-Drp1-S600A as indicated. Neurons (at 11 DIV) were then treated without (No sti) or with 45 mM K^+ for 15 min, and mitochondrial fluorescence was analyzed by time-lapse imaging. Bars, 10 μm. (E) Mitochondrial length was measured through analysis of the elongation index. Values shown are the mean ± SEM ($n = 5$) in each group. Values were analyzed using one-way ANOVA followed by post-Tukey test. *, $P < 0.05$; **, $P < 0.005$.

cells, we down-regulated Drp1 expression using RNAi and substituted expression with wild-type Drp1 or mutant Drp1 in which Ser600 was changed to alanine (S600A) to mimic the dephospho-state or to aspartic acid (S600D) to mimic the phospho-state (Fig. 6). The RNAi treatment reduced expression of endogenous Drp1 significantly, and the level of expression of the wild-type and mutant RNAi-resistant forms of YFP-Drp1 were slightly higher than that of the normal levels of the endogenous protein (Fig. 6 A). High K^+ treatment of HeLa cells also resulted in a rapid appearance of fragmented mitochondria in control cells or in cells in which endogenous Drp1 expression was reduced, although wild-type RNAi-resistant YFP-Drp1 or the YFP-Drp1-S600D mutant was expressed (Fig. 6, B and C). In contrast, expression of the RNAi-resistant YFP-Drp1-S600A resulted in attenuation of the effect of high K^+ treatment on mitochondrial fragmentation.

We also transfected neurons with pDsRed2-Mito and GFP, YFP-Drp1, or YFP-Drp1-S600A and examined mitochondrial morphology during K^+ stimulation. In these experiments, endogenous expression of Drp1 was not down-regulated with RNAi.

Published August 11, 2008

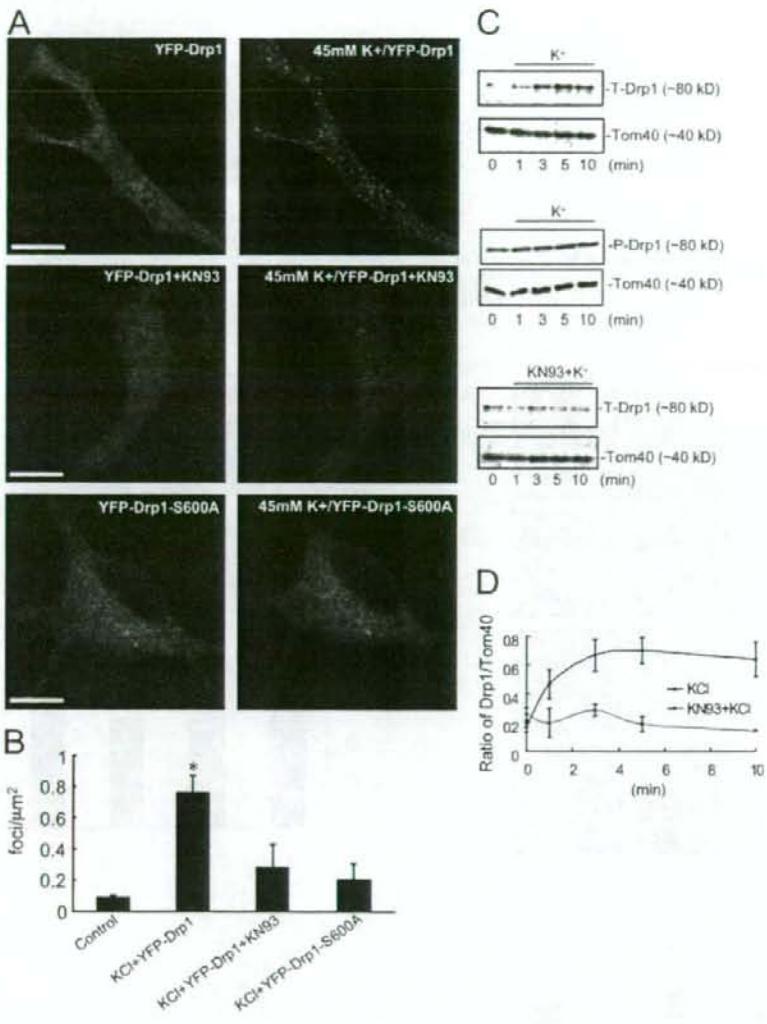

Figure 7. **CaMKIα-dependent phosphorylation regulates Drp1 intracellular distribution in neurons.** (A) Neurons (10 DIV) were transfected with YFP-Drp1 or YFP-Drp1-S600A. Neurons (at 11 DIV) were untreated (left) or treated with (right) 45 mM K^+ or preincubated with 20 μM KN93 for 30 min before high K^+ stimulation. Bars, 10 μm. (B) Quantitative analysis of exogenous Drp1 foci. Data were obtained from at least five independent experiments for each condition shown in A. Control is YFP-Drp1 without stimulation. Error bars indicate SD in each group. *, $P < 0.05$. (C) Neurons were treated with 45 mM K^+ in the absence or presence of 20 μM KN93 for various times as indicated. Proteins in mitochondrial fractions were separated by SDS-PAGE and analyzed by immunoblotting using Drp1 T-Drp1, P-Drp1, or Tom40 (for quantification of mitochondrial membrane) antibodies. (D) Quantitative analysis of Drp1 translocation. Drp1 levels were normalized to Tom40 levels at the time points indicated in Fig. 7 C. Cumulative results from three independent experiments for each condition are shown. Error bars indicate the mean ± SEM in each group.

As expected, high K^+ treatment of neurons transfected with GFP or wild-type YFP-Drp1 resulted in the rapid appearance of fragmented mitochondria throughout dendrites (Fig. 6, D and E). In contrast, expression of YFP-Drp1-S600A significantly inhibited the effects of high K^+ treatment on mitochondrial morphology.

Drp1's mitochondrial localization is regulated by CaMKIα-dependent phosphorylation

In mammalian cells, Drp1 is believed to translocate to the outer mitochondrial membrane, where it interacts with Fis1 and perhaps other proteins (Yoon et al., 2001). We transfected neurons with YFP-Drp1 and examined the localization of the protein (Fig. 7). Under control conditions, wild-type YFP-Drp1 was found evenly distributed throughout the cytoplasm (Fig. 7 A). High K^+ treatment resulted in the rapid appearance of punctate YFP-Drp1 staining throughout the cytoplasm (Fig. 7 A; quantitative analysis of exogenous Drp1 foci in neurons shown in Fig. 7 B). Preincubation with KN93 attenuated the appearance of the punctate YFP-Drp1 stain in response to high K^+ treatment (Fig. 7, A and B). In addition, high K^+ had no significant effect on the cytoplasmic localization of the mutant YFP-Drp1-S600A (Fig. 7, A and B). We also performed biochemical fractionation assays to examine the distribution of endogenous Drp1 after high K^+ stimulation. Phosphorylated Drp1 rapidly translocated to the mitochondrial fraction after high K^+ treatment, and this was blocked by pretreatment with KN93 (Fig. 7, C and D).

Similar studies were performed in HeLa cells in which endogenous Drp1 was down-regulated with RNAi and replaced by expression of either wild-type or mutant YFP-Drp1 (Fig. 8). High K^+ treatment also induced the rapid appearance of punctate YFP-Drp1 in HeLa cells (Fig. 8, A and B). This was accompanied by fragmentation of mitochondria (Fig. 6, A and B). Similar to neurons, high K^+ had no significant effect on the cytoplasmic localization of YFP-Drp1-S600A. However, somewhat unexpectedly,

Published August 11, 2008

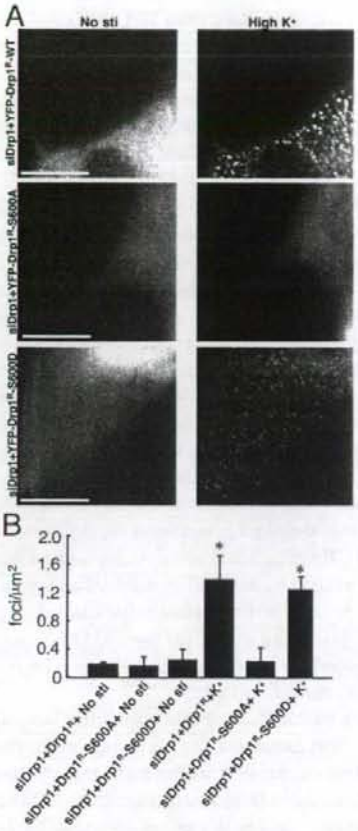

Figure 8. **High K^+ treatment regulates Drp1 dynamics in HeLa cells.** (A) HeLa cells were transfected with control siRNA (siCont) and siRNA for Drp1 (siDrp1) before the transfection with GFP, YFP-$Drp1^R$, or YFP-$Drp1^R$-S600A and mito-DsRed as described above. HeLa cells were then either untreated or incubated with 20 mM K^+ for 15 min. (B) Quantitative analysis of exogenous Drp1 foci. Data were obtained from the results from at least five independent experiments for each condition shown in A. Values were analyzed using one-way ANOVA followed by post-Turkey test. Control is siDrp1 without stimulation. Error bars indicate SD in each group. *, $P < 0.01$ versus siDrp1+YFP-$Drp1^R$+No stimulation. Bars, 10 μm.

the YFP-Drp1-S600D protein was found diffusely distributed in the cytosol under basal conditions, and high K^+ treatment also resulted in the rapid appearance of punctate staining of this phosphomimetic mutant protein.

In mammalian cells, Drp1 has been shown to regulate mitochondrial fission through an interaction with Fis1 (Yoon et al., 2003). Therefore, we examined in vitro whether CaMKIα-dependent phosphorylation of Drp1 could facilitate the interaction of Drp1 with hFis1. In the absence of prior phosphorylation by CaMKIα, a small amount of Drp1-6His was pulled down by GST-hFis1. Phosphorylation of wild-type Drp1 by CaMKIα resulted in a substantial increase in the amount of Drp1-6His pulled down by GST-hFis1 (Fig. 9 A). The amount of Drp1 bound to GST-Fis1 increased in proportion to the level of phosphorylation of Drp1 (Fig. 9 B). In contrast to wild-type Drp1, there was little measurable binding found between Drp1-S600A and GST-Fis1 (Fig. 9 C). Finally, after down-regulation of Fis1 with siRNA in HeLa cells, the effect of high K^+ on the punctate distribution of YFP-Drp1 was reduced (Fig. S3, available at http://www.jcb.org/cgi/content/full/jcb.200802164/DC1).

Discussion

In this study, we have demonstrated that Ca^{2+}-dependent signaling has profound effects on mitochondrial dynamics. The regulation of mitochondrial dynamics in response to high K^+ stimulation involved activation of N-type VDCCs, P/Q-type VDCCs, and, to a lesser degree, L-type VDCCs and subsequent Ca^{2+} entry into cells. In response to VDCC activation, mitochondria exhibit significant morphological and dynamic changes. Mitochondria very rapidly stopped moving and formed ringlike structures that accompanied the division process. An elongated mitochondrial morphology was rapidly recovered, and neuronal viability was not impaired after washout of high K^+ from the medium. These results were obtained from studies using live-cell imaging with mitochondrial-targeted fluorescent protein as well as by electron microscopy. The electron micrographs showed that the high K^+ treatment resulted in mitochondria that appeared hollow with a less electron-dense matrix and less cristae. The ringlike formation and hollow mitochondrial changes during fission are also consistent with results from studies in which hFis1 was overexpressed in HeLa cells (Yoon et al., 2003).

The effect of Ca^{2+} on mitochondrial movement and morphology required the activity of CaMKI. KN93, a CaMK inhibitor known to inhibit CaMKI in neurons, almost completely blocked the effects of high K^+ on mitochondrial dynamics. More specifically, expression of CaMKIα-DN blocked the effect of high K^+ on mitochondrial movement and morphology, although CaMKIα-CA mimicked the effects of high K^+. Moreover, our experiments indicated that phosphorylation of Drp1 by CaMKIα was likely to play an important role in the effect of high K^+. Our results indicated that Ca^{2+} influx via VDCCs resulted in activation of CaMKIα and the phosphorylation of Drp1 at Ser600. Ser600 is included within a consensus CaMKI phosphorylation site in the C-terminal GTPase effector domain (GED; Fig. S2 A). In contrast to dynamin, Drp1 does not have a pleckstrin homology domain, and the GED is necessary and sufficient for interaction with mitochondria (Pitts et al., 2004). The GED is conserved in all Drp1 isoforms, and all are likely to be regulated by CaMKIα-dependent phosphorylation.

The recruitment of Drp1 to the cytoplasmic side of the outer mitochondrial membrane is dependent on Fis1 (Yoon et al., 2003). Fis1 is a small 17-kD protein that interacts with the outer mitochondrial membrane via its C terminus (Mozdy et al., 2000) and interacts with Drp1 via two N-terminal tetratricopeptide repeat motifs (Yu et al., 2005). The expression level of Fis1 appears to be the rate-limiting factor in mitochondrial fission through its ability to interact with Drp1 and recruit it in an active conformation to allow scission of the mitochondrial membrane. Our results showed that in intact cells, phosphorylation of Drp1 by CaMKIα was necessary for translocation of the protein to mitochondria. In addition, expression of a (dephospho) mutant Drp1 in which Ser600 was changed to alanine was able to attenuate the effect of high K^+ on mitochondrial morphology.

Published August 11, 2008

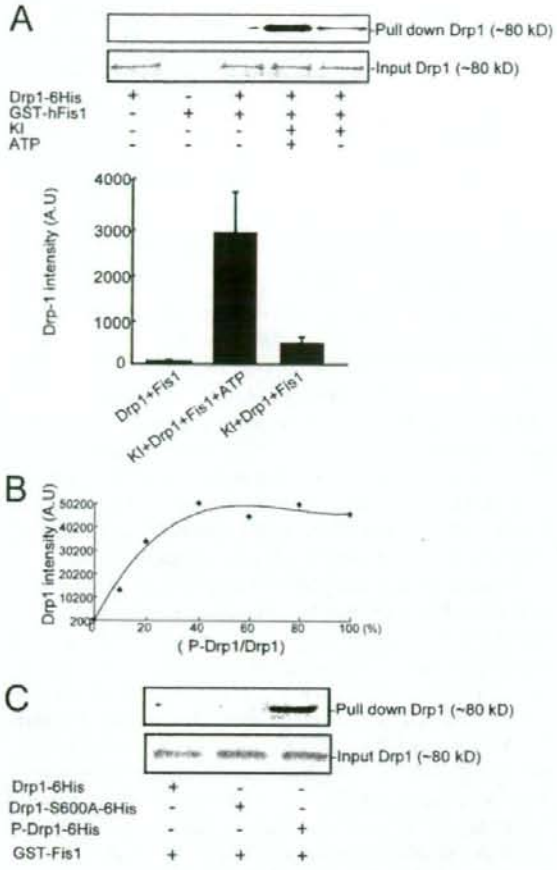

Figure 9. **Phosphorylation regulates Drp1 and hFis1 binding in vitro.** (A) Recombinant Drp1-6His was preincubated in the absence or presence of CaMKIα (KI) and ATP and mixed with GST-hFis1 as indicated. Proteins were recovered using glutathione-Sepharose and analyzed by immunoblotting using an anti-6His antibody to detect Drp1 (top; bottom shows Drp1 input). Quantitation of the results is shown in the bar graph. The results were otained in three independent experiments. Error bars indicate SEM in each group. (B) Drp1-6His was maximally phosphorylated by CaMKI, and the sample was mixed in different ratios with non-phosphorylated Drp1-6His (values are expressed as percent P-Drp1/Drp1; see x axis). GST pull-down assays were performed as in A. The data represent means from three independent experiments. (C) The binding of mutant Drp1-S600A-6His to GST-hFis1 was compared with unphosphorylated and phosphorylated wild-type Drp1-6His. Drp1 was detected by immunoblotting as described above. Similar results were obtained from two independent experiments.

Moreover, in vitro, prior phosphorylation of Drp1 by CaMKIα significantly increased the binding of Drp1 and Fis1. Finally, reduction of Fis1 expression was able to attenuate the effect of high K^+ on Drp1 translocation. Together, these results suggest that activation of CaMKIα and phosphorylation of Drp1 are necessary for the increased mitochondrial fission observed after exposure of cells to high K^+. Interestingly, a mutant Drp1 in which Ser600 was changed to aspartate to mimic the phosphorylated state behaved like the wild-type protein under basal and high K^+ conditions. This result indicates that the S600D mutation does not mimic phosphorylation by CaMKI and also suggests that CaMKI likely regulates the function of other proteins involved in Drp1 translocation to mitochondria.

Drp1 and Fis1 were found previously to interact by fluorescence resonance energy transfer and coimmunoprecipitation experiments. The proteins can also interact in vitro (Yoon et al., 2003). However, this interaction is normally transient (Wasiak et al., 2007), requiring the use of a chemical cross-linker to observe coimmunoprecipitation or interaction in vitro (Yoon et al., 2003). The precise molecular details of the interaction of Drp1 and Fis1 remain to be established. A study in yeast suggests that a third protein termed Mdv1 is required for the interaction between Dnm1 and Fis1 (Hoppins et al., 2007). However, a recent study suggests that *Saccharomyces cerevisiae* Fis1 directly binds Dnm1 and not Mdv1 in vitro (Wells et al., 2007). Interestingly, this binding is negatively regulated by a short N-terminal region of *S. cerevisiae* Fis1. Notably, the N-terminal region of Fis1 is not well conserved between yeast and mammals. Moreover, Mdv1 is not found in mammalian cells, and human Fis1 does not rescue deletion of the yeast gene (Suzuki et al., 2003; Stojanovski et al., 2004). Together, these observations suggest that the interactions between Drp1 and Fis1 in mammalian cells may be distinct from those occurring between the equivalent proteins in yeast. Phosphorylation of Drp1 by CaMKIα may therefore represent a mechanism by which the affinity of Drp1 and Fis1 is increased in mammalian cells.

During the revision of this manuscript, several other recent studies also found that Drp1 is phosphorylated in mammalian cells. Two independent studies found that cAMP-dependent PKA phosphorylated Drp1 at the same site as CaMKI (different residue numbers reflect the use of different Drp1 isoforms; Chang and Blackstone, 2007; Cribbs and Strack, 2007). CaMKI and PKA are known to have overlapping substrate specificity and, for example, phosphorylation of a common serine residue in synapsin I has been found to be phosphorylated in response to high K^+ treatment or increased cAMP levels (Nairn and Greengard, 1987). Although there were some differences between the two studies, there was a general agreement on the conclusion. Results obtained from the use of phosphosite mutants of Drp1 indicated that increased phosphorylation of Drp1 was associated with increased mitochondrial length or area, results consistent with decreased mitochondrial fission. Moreover, the study by Cribbs and Strack (2007) found that expression of a phosphomimetic form of Drp1 was associated with increased resistance to proapoptotic treatments. These studies did not find any effect of phosphorylation on Drp1 self-assembly.

The basis for the difference between our study and these two recent studies is not clear (Chang and Blackstone, 2007; Cribbs and Strack, 2007). It is notable, however, that there was general agreement that the basal level of phosphorylation of native Drp1 was very low. Based on the results from these two studies, a low level of phosphorylation of Drp1 would predict that mitochondria would be expected to be highly fragmented and cells would be vulnerable to apoptosis. However, this situation is generally the opposite of what was actually observed. In our studies, mitochondria were highly elongated, especially in neuronal dendrites, consistent with the idea that a low basal

Published August 11, 2008

phosphorylation of Drp1 favors mitochondrial fusion and increased phosphorylation favors mitochondrial fission. Another notable feature of these two studies is that they did not find any effect of increased cAMP levels on mitochondrial morphology. This result is consistent with the idea that phosphorylation of Drp1 at Ser600, although necessary for regulation of mitochondrial morphology, is not sufficient on its own and that activation of CaMKI has additional roles in regulation of Drp1 interaction with mitochondria. It will be interesting to investigate whether Ca^{2+}- and cAMP-dependent signaling pathways can act synergistically to regulate mitochondrial morphology.

Another recent study found that rat Drp1 is phosphorylated by Cdk1/cyclin B, leading to stimulation of mitochondrial fission during mitosis (Taguchi et al., 2007). The CaMKIα and Cdk1 phosphorylation sites are very close in the C terminus of Drp1, highlighting the important role of this region of the protein in regulation of mitochondrial fission. Phosphorylation at the C terminus, at least in the case of CaMKIα, presumably results in alterations in the conformation of Drp1 and increases affinity of Drp1 for Fis1. It will be of interest to investigate whether phosphorylation of Drp1 by Cdk1 also stimulates fission through an increase in its affinity for Fis1 and to examine the interrelationship between the phosphorylation of these sites.

Recent studies have found that mitochondria distribution and movement in dendrites is regulated by synaptic activity (Li et al., 2004; Chang and Reynolds, 2006; Sung et al., 2008). K^+-dependent depolarization or titanic stimulation was associated with a redistribution of mitochondria to dendritic spines, presumably to support the high metabolic requirement at these sites during synaptic activation. Moreover, increased Drp1 activity was found to be associated with increased mitochondrial fission, redistribution of mitochondria to dendrites, density of dendritic spines, and synaptic activity (Li et al., 2004). Preferential activation of CaMKs is found with protocols that increase long-term potentiation at excitatory synapses (Xia and Storm, 2005). CaMKIα-dependent phosphorylation of Drp1 and altered mitochondrial dynamics are therefore likely to play an important role in changes in synaptic morphology and function that accompany long-term potentiation.

Our results indicated that the effects of high K^+ treatment were rapid, occurring within minutes, and were reversible. Moreover, high K^+ treatment had no effect on cell death. This latter finding is of interest because several previous studies have suggested that mitochondrial fission is involved in cell death (Frank et al., 2001; Fannjiang et al., 2004; Lee et al., 2004; Youle and Karbowski, 2005). In particular, Drp1 has been found to be associated with proapoptotic members of the Bcl-2 family at sites of membrane scission during apoptosis (Wasiak et al., 2007). However, recent studies have also suggested that mitochondrial fission, although necessary for certain types of cell death, is not itself sufficient to cause apoptosis (Szabadkai et al., 2004; Meuer et al., 2007). The results of the current study add support to this hypothesis. Indeed, in preliminary experiments, we found that pretreatment with high K^+ in neurons could prevent release of cytochrome *c* from mitochondria and prevent apoptosis in response to glutamate treatment (unpublished data). CaMKIα-dependent phosphorylation of Drp1 may play an important role in this protective process.

In conclusion, these results provide important new insights into the understanding of intracellular signaling pathways that regulate mitochondrial dynamics and morphology. We found that mitochondrial dynamics and morphology are controlled by Ca^{2+} influx through VDCCs. In turn, VDCCs are coupled to the activation of CaMKIα, resulting in phosphorylation of Drp1. CaMKIα-dependent phosphorylation of Drp1 facilitates its interaction with Fis1 and leads to increased mitochondrial fission. In addition to the phosphorylation of Drp1, CaMKIα may also influence other aspects of Drp1 translocation to mitochondria. Mitochondrial morphology is regulated by a balance between fission and fusion. Although we cannot rule out the possibility that mitochondrial fragmentation induced by high K^+ is also accompanied by inhibition of mitochondrial fusion, the results indicate that the effects of high K^+ are mediated by activation of CaMKI and phosphorylation of Drp1. This suggests that the fission process is the most likely target for the effects of high K^+. Although our studies focused on regulation of Drp1 in neurons, we also found that CaMKI could regulate Drp1 function in HeLa cells. Ca^{2+} release from the ER has also been found to promote the translocation of Drp1 from the cytoplasm to the outer mitochondrial membrane of nonneuronal cells (Breckenridge et al., 2003). CaMKI is a ubiquitously expressed protein kinase. Thus, CaMKI-dependent phosphorylation and regulation of Drp1 may be a general phenomenon found in many different types of cells.

Materials and methods

DNA construction

PDsRed2-Mito (Clontech Laboratories, Inc.) is a mammalian expression vector that encodes the fluorescent protein DsRed2 tagged with the mitochondrial targeting sequence from subunit VIII of human cytochrome *c* oxidase. CaMKIα-DN was generated by mutating K49 to E to disrupt catalytic activity. CaMKIα-CA was obtained by truncating the autoinhibitory and CaM-binding domains (Yokokura et al., 1995; Matsushita and Nairn, 1998). The wild-type Drp1 (isoform 3) plasmid was provided by A.M. van der Bliek (University of California, Los Angeles, Los Angeles, CA; Smirnova et al., 1998). Drp1-S600A and S600D site-directed mutagenesis was performed using a Quickchange kit (Stratagene) according to the manufacturer's instructions. To replace endogenous Drp1 with RNAi-resistant YFP-Drp1, the underlined nucleotide T was changed to C to introduce a silent mutation in the Drp1 siRNA target sequence (1417-CGTAAAAGGTTGCCTGTTACA). Wild-type Drp1 and Drp1-S600A were cloned into pGEX-6p-1 and PET 21a+ for GST-Drp1 and Drp1-6His protein purification, respectively. CaMKK-433 and CaMKI-293 were also cloned into PET 21a+ for recombinant protein purification as described previously (Matsushita and Nairn, 1998). hFis1 cDNA was cloned by RT-PCR from HeLa cells. hFis1-ΔC (without 30 amino acids at the C terminus) was cloned into the pGEX-6p-1 vector for GST–hFis1-C protein purification.

Primary neuronal culture

The hippocampus from ~18–19-embryonic day fetal Wistar rats was treated with 0.125% trypsin (Invitrogen) and 0.004% DNase-I (Sigma-Aldrich) at 37°C for 15 min and mechanically dissociated. Neurons were plated on poly-L-lysine (Sigma-Aldrich) and laminin (Roche)-coated glass-bottomed or plastic-bottomed 35-mm culture dishes (cell density was ~25,000–30,000/35-mm dish for microscopy or ~45,000–50,000/35-mm dish for Western blotting). Cells were maintained in culture medium with DME, 100 μg/ml penicillin-streptomycin (Invitrogen), and 10% fetal calf serum (Invitrogen). Cultures were maintained at 37°C in a 95% air, 5% CO_2 humidified incubator. On the second day, the culture medium was replaced with medium containing DME, 2% B-27 supplement (Invitrogen), and 5% fetal calf serum. On the fourth day, the culture medium was replaced

Published August 11, 2008

with medium containing DME, α-MEM, F-12 nutrient mixture, 2% B-27 supplement, 0.34% glucose, 25 μM 5-fluoro-deoxyuridine, 25 μM uridine, 1 mM kynurenic acid (Sigma-Aldrich), and 1% fetal calf serum. Cultures were used for experiments on days 9–12.

Transfection procedures

Transfection for neurons was performed with Lipofactamine 2000 (Invitrogen) according to the manufacturer's instructions. After 6 h of incubation, the medium containing Lipofactamine was replaced with normal culture medium. The cells were viewed 18–24 h after transfection by fluorescence microscopy. Predesigned siRNA for human CaMKIα (Thermo Fisher Scientific), human Fis1 (Thermo Fisher Scientific), and human Drp1 (Sigma-Aldrich) was introduced with DharmaFECT Transfection reagents according to the manufacturer's instructions.

Time-lapse imaging of mitochondria or Drp1

Mitochondrial imaging was performed with an inverted fluorescence microscope (Axiovert 200; Carl Zeiss, Inc.) with excitation at 545 nm using neuronal culture medium or DME (Invitrogen) with 10% FBS at 30°C. Illumination and exposure to the CCD camera (ORCA; Hamamatsu Photonics) were controlled and synchronized with AquaCosmos software (Hamamatsu Photonics). 63×/1.4 NA (Plan Apochromat; Carl Zeiss, Inc.) or 100×/1.45 NA (Plan Fluar; Carl Zeiss, Inc.) objectives were used to view the cells, and a narrow bandpass rhodamine filter was used when capturing the fluorescence images. GFP was visualized with excitation at 480 nm using an FITC filter. Time-lapse imaging was captured automatically with a selected interval. Drp1 imaging was performed with a laser confocal microscope (Fluoview 300; Olympus). 60×/1.0 NA or 40×/0.9 NA WLSM (PlauApo) objectives (Olympus) were used to view the cells. YFP or GFP was visualized using a BA 505–525 barrier filter. Mito-DsRed was viewed using a BA 565IF filter. Time-lapse imaging was also captured automatically with a selected interval. To analyze Drp1 foci, we selected random regions in neurons. The areas of these regions were also different in different cells, but their areas (micrometers squared) were automatically calculated by the software (Fluoview 300; Olympus). The background was then subtracted, and the number of Drp1 foci was counted and divided by the area to obtain foci/micrometers squared for Drp1 distribution in cells.

Analysis of mitochondrial movement and morphology

AquaCosmos software (Hamamatsu Photonics) was used to analyze mitochondrial movement and morphology. Mitochondrial movement was evaluated by analyzing the pDsRed2-Mito signal with time-lapse imaging using neuronal culture medium or DME (Invitrogen) with 10% FBS at 30°C. Pixel intensity difference was obtained by image subtraction between successive images at 10-s intervals, and the difference after subtraction of the background was calculated as the movement during the 10-s period. Image differences between six sequential images were averaged. The pixel area of the image was normalized to the total mitochondrial pixel area before subtraction. Morphology was evaluated by elongation index. Mitochondria were picked up after subtraction of background by using AquaCosmos software (Hamamatsu Photonics). The length and the area of an individual mitochondria were measured, and the elongation index was calculated by the square of the length divided by the area (i.e., when the elongation index is larger, mitochondria are longer). The elongation index after 15 min of high K^+ stimulation was normalized to the value measured before stimulation to obtain the percent change in elongation index.

Intracellular Ca^{2+} measurement

Hippocampal cultures were incubated with Fura-2 AM (5 μM for 30 min) and washed with Hepes-buffered salt solution composed of 119 mM NaCl, 2.5 mM KCl, 2 mM $CaCl_2$, 2 mM $MgCl_2$, and 20 mM glucose in 25 mM Hepes (buffered to pH 7.4 with NaOH) at 30°C. Ca^{2+} measurement was performed with an epifluorescence inverted microscope (Axiovert 200; Carl Zeiss, Inc.) equipped with a 20×/NA 0.75 Fluar UV objective and Ca^{2+} ratio imaging system (Hamamatsu Photonics). Ratiometric measurement of Fura-2 fluorescence was obtained by sequential excitation at 340- and 380-nm lights from a xenon arc lamp. The intracellular Ca^{2+} change was indicated as the ratio of emitted fluorescence at 340- and 380-nm excitations.

Neuronal cell death assay

Hippocampal neuronal cultures were exposed to 500 μM glutamate or 45 mM of high K^+ for15 min. After treatment, the cultures were washed and incubated with normal media taken from a batch of neurons cultured in parallel. After 24 h of incubation, the cultures were fixed with 4% PFA for 10 min. Cultures were stained with MAP2 antibody and Hoechst 33258 and analyzed by an inverted fluorescence microscope (Axiovert 200; Carl Zeiss, Inc.) using a 20×/0.75 NA Fluar objective. Neurons with condensed Hoechst 33258 staining were counted as dead cells.

Electron microscopy

Hippocampal neurons cultured on glass coverslips were washed with 0.1 M sodium cacodylate buffer, pH 7.4, and fixed with 2% glutaraldehyde and 3% PFA in 0.1 M sodium cacodylate buffer. After washing in 0.1 M sodium cacodylate buffer, the neurons were postfixed with 2% OsO_4 in the same buffer, block stained in 2% aqueous uranyl acetate, dehydrated in ascending alcohols and propylene oxide, and finally embedded in epoxy resin Quetol 812 (Nisshin EM Co.) between a Teflon support and the coverglass. After Quetol 812 polymerization, the coverglass was removed by dipping the sample alternatively into liquid nitrogen and hot water. Neurons to be sectioned were selected by observing the flat-embedded resin plate under the light microscope. Areas containing the selected neurons were cut out and mounted on resin blocks for thin sectioning. 60–70-nm sections were stained with 2% aqueous uranyl acetate and lead citrate, and micrographs were taken at 75 kV in a transmission electron microscope (H-7100; Hitachi).

Purification of recombinant proteins

Purification of recombinant proteins was performed as described previously (Matsushita and Nairn, 1998). In brief, BL21 cells containing each expression plasmid were grown overnight at 37°C. The proteins were expressed in these cells after induction with 0.2 mM isopropyl1-thio-β-D-galactopyranoside. The expressed proteins were purified using a column of glutathione–Sepharose 4 Fast Flow (GE Healthcare) for GST proteins or Probond Nickel-Chelating resin (Invitrogen) for 6His-tagged proteins. Fractions were collected, and protein was analyzed by SDS-PAGE and staining with Coomassie brilliant blue. Fractions containing expressed protein were pooled and dialyzed against PBS. Protein concentrations were determined using a protein assay kit (Bio-Rad Laboratories). Aliquots were stored at −80°C.

Phosphorylation assays

The CaMK kinase assay buffer (100 μl) contained 50 mM Hepes, pH 7.5, 10 mM magnesium acetate, 1 mM EGTA, 5 mM dithiothreitol, 2.4 μM calmodulin, and 2 mM $CaCl_2$. For CaMKII assays, 20 mM Hepes, pH 7.4, 10 mM $MgCl_2$, and 1 mM dithiothreitol were used. The final concentrations of kinases or proteins were 500 ng/ml CaMKKα-433-6His, 1 μg/ml CaMKIα-293-6His, and 10 μg/ml CaMKII, GST-Drp1, or GST-Drp1-S600A. Reactions were initiated by the addition of γ-[^{32}P]ATP (100 μM; 2–5 × 10^2 cpm/pmol) and incubated at 30°C for 30 min. Reactions were terminated by the addition of 100 μl SDS sample buffer (1% SDS, 60 mM Tris-HCl, pH 6.8, 5% [vol/vol] glycerol, and 0.2 M β-mercaptoethanol) and boiling at 100°C for 5 min. Samples were analyzed by SDS-PAGE (8% polyacrylamide) and autoradiography. For samples analyzed by immunoblotting, γ-[^{32}P]ATP was replaced by nonradioactive ATP.

Drp1 phosphospecific antibody

A peptide corresponding to residues 594–608 of Drp1-3 (PVARKLS(p) AREQRDCE) was chemically phosphorylated at residue Ser600, and a rabbit polyclonal antibody was generated by Genosys (Sigma-Aldrich) essentially as described previously (Tomizawa et al., 2003).

Immunoblotting

After treatment of cultured neurons (9–12 days in vitro [DIV]), dishes were washed once with ice-cold PBS, and adherent cells were scraped with lysis buffer A (20 mM Tris, pH 7.4, 150 mM NaCl, 10 mM sodium orthovanadate, 20 mM sodium fluoride, 0.25 M sucrose, 1 mM dithiothreitol, 500 nM okadaic acid, and 0.5% Tween 20). Cell lysates were sonicated in 4× sample buffer, boiled for 5 min, and stored at −20°C until used. Proteins were analyzed by SDS-PAGE and immunoblotting on nitrocellulose membranes. Total Drp1 was probed with Drp1 monoclonal antibody (1:1,000 dilution; BD Biosciences), and phosphorylated Drp1 was probed with phospho-Ser600 antibody (1:1,000), both at 4°C overnight. HRP-conjugated secondary antibody was used at 1:2,000, and blotting signals were detected with standard protocols.

GST pull-down experiments

10 μg/ml of recombinant 6His-tagged Drp1 was phosphorylated by CaMKIα as described above using nonradioactive ATP. After incubation for 60 min at 30°C, 10 μg/ml GST-hFis1 was added followed by GST–Sepharose beads

Published August 11, 2008

in the presence of PBS, pH 7.4, 1% BSA, and 0.1% Tween 20. Samples were mixed by gentle shaking at 4°C for at least 2 h and washed four times in washing buffer (20 mM Tris-HCl, pH 7.4, 500 mM NaCl, and 1% Tween 20). The GST beads were collected, proteins were eluted with sample buffer, and samples were analyzed by SDS-PAGE and immunoblotting. Drp1 bound to GST-hFis1 was detected with anti-6His monoclonal antibody (mouse IgG1, 1:5,000; BD Biosciences). For binding kinetics analysis, phosphorylated Drp1-6His was prepared as described above. The phosphorylated Drp1 was then mixed in different ratios with non-phosphorylated Drp1, and the percentage of Drp1-P relative to the total Drp1 was calculated. Drp1-6His bound to GST-Fis1 was detected by immunoblotting analysis.

Preparation of mitochondria-enriched fractions

Plated neurons were washed once with ice-cold PBS and scraped in lysis buffer A (20 mM Tris, pH 7.4, 150 mM NaCl, 10 mM sodium orthovanadate, 20 mM sodium fluoride, 0.25 M sucrose, 1 mM dithiothreitol, 500 nM okadaic acid, Complete 1 tablet/50 ml lysis buffer A, and 0.5% Tween 20). Cells were lysed by passing them 10 times through a 28-G 1/2 needle and centrifuged at 1,300 *g* for 15 min to remove nuclei and unbroken cells. The supernatant was collected and centrifuged again for 15 min at 5,000 *g* to pellet the mitochondria-enriched fraction. The mitochondrial pellets were diluted with 4× sample buffer, boiled for 6 min at 100°C, and stored at −30°C. The mitochondria membrane protein Tom40 was blotted (rabbit polyclonal antibody; Santa Cruz Biotechnology, Inc.) and used as an endogenous control.

Statistical analysis

The significance between the experimental groups was assessed by using one-way analysis of variance (ANOVA) followed by post-Tukey test. For single comparison, we performed an unpaired Student's *t* test. Data are shown as the mean ± SEM, and $P < 0.05$ was considered significant.

Online supplemental material

Fig. S1 shows that high K^+ treatment alters mitochondrial movement in neurons. Fig. S2 shows a conserved phosphorylation CaMKI/PKA consensus motif in Drp1 proteins and down-regulation of CaMKIα level expression using RNAi. Fig. S3 shows that Fis1 regulates K^+-induced Drp1 intracellular distribution in HeLa cells. Online supplemental material is available at http://www.jcb.org/cgi/content/full/jcb.200802164/DC1.

We are grateful to A.M. van der Bliek for Drp1 plasmids. We thank T. Ogawa for technical assistance.

This work was supported in part by grants-in-aid for scientific research from the Ministry of Education, Culture, Sports, Science and Technology of Japan; by grants from Preventure-Japan Science and Technology Agency; and by the National Institutes of Health (A.C. Nairn).

Submitted: 26 February 2008
Accepted: 15 July 2008

References

Barsoum, M.J., H. Yuan, A.A. Gerencser, G. Liot, Y. Kushnareva, S. Graber, I. Kovacs, W.D. Lee, J. Waggoner, J. Cui, et al. 2006. Nitric oxide-induced mitochondrial fission is regulated by dynamin-related GTPases in neurons. *EMBO J.* 25:3900–3911.

Bereiter-Hahn, J., and M. Voth. 1994. Dynamics of mitochondria in living cells: shape changes, dislocations, fusion, and fission of mitochondria. *Microsc. Res. Tech.* 27:198–219.

Bossy-Wetzel, E., M.J. Barsoum, A. Godzik, R. Schwarzenbacher, and S.A. Lipton. 2003. Mitochondrial fission in apoptosis, neurodegeneratin and aging. *Curr. Opin. Cell Biol.* 15:706–716.

Breckenridge, D.G., M. Stojanovic, R.C. Marcellus, and G.C. Shore. 2003. Caspase cleavage product of BAP31 induces mitochondrial fission through endoplasmic reticulum calcium signals, enhancing cytochrome *c* release to the cytosol. *J. Cell Biol.* 160:1115–1127.

Cerveny, K.L., Y. Tamura, Z. Zhang, R.E. Jensen, and H. Sesaki. 2007. Regulation of mitochondrial fusion and division. *Trends Cell Biol.* 17:563–569.

Chada, S.R., and P.J. Hollenbeck. 2003. Mitochondrial movement and positioning in axons: the role of growth factor signaling. *J. Exp. Biol.* 206:1985–1992.

Chan, D.C. 2006. Mitochondrial fusion and fission in mammals. *Annu. Rev. Cell Dev. Biol.* 22:79–99.

Chang, C.R., and C. Blackstone. 2007. Cyclic AMP-dependent protein kinase phosphorylation of Drp1 regulates its GTPase activity and mitochondrial morphology. *J. Biol. Chem.* 282:21583–21587.

Chang, D.T., and I.J. Reynolds. 2006. Differences in mitochondrial movement and morphology in young and mature primary cortical neurons in culture. *Neuroscience.* 141:727–736.

Cribbs, J.T., and S. Strack. 2007. Reversible phosphorylation of Drp1 by cyclic AMP-dependent protein kinase and calcineurin regulates mitochondrial fission and cell death. *EMBO Rep.* 8:939–944.

Detmer, S.A., and D.C. Chan. 2007. Functions and dysfunctions of mitochondrial dynamics. *Nat. Rev. Mol. Cell Biol.* 8:870–879.

Fannjiang, Y., W.C. Cheng, S.J. Lee, B. Qi, J. Pevsner, J.M. McCaffery, R.B. Hill, G. Basanez, and J.M. Hardwick. 2004. Mitochondrial fission proteins regulate programmed cell death in yeast. *Genes Dev.* 18:2785–2797.

Frank, S., B. Gaume, E.S. Bergmann-Leitner, W.W. Leitner, E.G. Robert, F. Catez, C.L. Smith, and R.J. Youle. 2001. The role of dynamin-related protein 1, a mediator of mitochondrial fission, in apoptosis. *Dev. Cell.* 1:515–525.

Hook, S.S., and A.R. Means. 2001. Ca(2+)/CaM-dependent kinases: from activation to function. *Annu. Rev. Pharmacol. Toxicol.* 41:471–505.

Hoppins, S., L. Lackner, and J. Nunnari. 2007. The machines that divide and fuse mitochondria. *Annu. Rev. Biochem.* 76:751–780.

Karbowski, M., K.L. Norris, M.M. Cleland, S.Y. Jeong, and R.J. Youle. 2006. Role of Bax and Bak in mitochondrial morphogenesis. *Nature.* 443:658–662.

Kroemer, G., and J.C. Reed. 2000. Mitochondrial control of cell death. *Nat. Med.* 6:513–519.

Lee, J.C., Y.G. Kwon, D.S. Lawrence, and A.M. Edelman. 1994. A requirement of hydrophobic and basic amino acid residues for substrate recognition by Ca^{2+}/calmodulin-dependent protein kinase Ia. *Proc. Natl. Acad. Sci. USA.* 91:6413–6417.

Lee, Y.J., S.Y. Jeong, M. Karbowski, C.L. Smith, and R.J. Youle. 2004. Roles of the mammalian mitochondrial fission and fusion mediators Fis1, Drp1, and Opa1 in apoptosis. *Mol. Biol. Cell.* 15:5001–5011.

Li, Z., K. Okamoto, Y. Hayashi, and M. Sheng. 2004. The importance of dendritic mitochondria in the morphogenesis and plasticity of spines and synapses. *Cell.* 119:873–887.

Ligon, L.A., and O. Steward. 2000. Movement of mitochondria in the axons and dendrites of cultured hippocampal neurons. *J. Comp. Neurol.* 427:340–350.

Matsushita, M., and A.C. Nairn. 1998. Characterization of the mechanism of regulation of Ca^{2+}/calmodulin-dependent protein kinase I by calmodulin and by Ca^{2+}/calmodulin-dependent protein kinase kinase. *J. Biol. Chem.* 273:21473–21481.

Meuer, K., I.E. Suppanz, P. Lingor, V. Planchamp, B. Goricke, L. Fichtner, G.H. Braus, G.P. Dietz, S. Jakobs, M. Bahr, and J.H. Weishaupt. 2007. Cyclin-dependent kinase 5 is an upstream regulator of mitochondrial fission during neuronal apoptosis. *Cell Death Differ.* 14:651–661.

Mozdy, A.D., J.M. McCaffery, and J.M. Shaw. 2000. Dnm1p GTPase-mediated mitochondrial fission is a multi-step process requiring the novel integral membrane component Fis1p. *J. Cell Biol.* 151:367–380.

Nairn, A.C., and P. Greengard. 1987. Purification and characterization of Ca^{2+}/calmodulin-dependent protein kinase I from bovine brain. *J. Biol. Chem.* 262:7273–7281.

Oakes, S.A., and S.J. Korsmeyer. 2004. Untangling the web: mitochondrial fission and apoptosis. *Dev. Cell.* 7:460–462.

Pitts, K.R., M.A. McNiven, and Y. Yoon. 2004. Mitochondria-specific function of the dynamin family protein DLP1 is mediated by its C-terminal domains. *J. Biol. Chem.* 279:50286–50294.

Rube, D.A., and A.M. van der Bliek. 2004. Mitochondrial morphology is dynamic and varied. *Mol. Cell. Biochem.* 256-257:331–339.

Ruthel, G., and P.J. Hollenbeck. 2003. Response of mitochondrial traffic to axon determination and differential branch growth. *J. Neurosci.* 23:8618–8624.

Schmitt, J.M., E.S. Guire, T. Saneyoshi, and T.R. Soderling. 2005. Calmodulin-dependent kinase kinase/calmodulin kinase I activity gates extracellular-regulated kinase-dependent long-term potentiation. *J. Neurosci.* 25:1281–1290.

Shaw, J.M., and J. Nunnari. 2002. Mitochondrial dynamics and division in budding yeast. *Trends Cell Biol.* 12:178–184.

Smirnova, E., D.L. Shurland, S.N. Ryazantsev, and A.M. van der Bliek. 1998. A human dynamin-related protein controls the distribution of mitochondria. *J. Cell Biol.* 143:351–358.

Smirnova, E., L. Griparic, D.L. Shurland, and A.M. van der Bliek. 2001. Dynamin-related protein Drp1 is required for mitochondrial division in mammalian cells. *Mol. Biol. Cell.* 12:2245–2256.

Stojanovski, D., O.S. Koutsopoulos, K. Okamoto, and M.T. Ryan. 2004. Levels of human Fis1 at the mitochondrial outer membrane regulate mitochondrial morphology. *J. Cell Sci.* 117:1201–1210.

Sung, J.Y., O. Engmann, M.A. Teylan, A.C. Nairn, P. Greengard, and Y. Kim. 2008. WAVE1 controls neuronal activity-induced mitochondrial distribution in dendritic spines. *Proc. Natl. Acad. Sci. USA.* 105:3112–3116.

Suzuki, M., S.Y. Jeong, M. Karbowski, R.J. Youle, and N. Tjandra. 2003. The solution structure of human mitochondria fission protein Fis1 reveals a novel TPR-like helix bundle. *J. Mol. Biol.* 334:445–458.

Szabadkai, G., A.M. Simoni, M. Chami, M.R. Wieckowski, R.J. Youle, and R. Rizzuto. 2004. Drp-1-dependent division of the mitochondrial network blocks intraorganellar Ca^{2+} waves and protects against Ca^{2+}-mediated apoptosis. *Mol. Cell.* 16:59–68.

Taguchi, N., N. Ishihara, A. Jofuku, T. Oka, and K. Mihara. 2007. Mitotic phosphorylation of dynamin-related GTPase Drp1 participates in mitochondrial fission. *J. Biol. Chem.* 282:11521–11529.

Takei, K., P.S. McPherson, S.L. Schmid, and P. De Camilli. 1995. Tubular membrane invaginations coated by dynamin rings are induced by GTP-γ S in nerve terminals. *Nature.* 374:186–190.

Tang, Y., and R. Zucker. 1997. Mitochondrial involvement in post-tetanic potentiation of synaptic transmission. *Neuron.* 18:483–491.

Tomizawa, K., S. Sunada, Y.F. Lu, Y. Oda, M. Kinuta, T. Ohshima, T. Saito, F.Y. Wei, M. Matsushita, S.T. Li, et al. 2003. Cophosphorylation of amphiphysin I and dynamin I by Cdk5 regulates clathrin-mediated endocytosis of synaptic vesicles. *J. Cell Biol.* 163:813–824.

Tondera, D., F. Czauderna, K. Paulick, R. Schwarzer, J. Kaufmann, and A. Santel. 2005. The mitochondrial protein MTP18 contributes to mitochondrial fission in mammalian cells. *J. Cell Sci.* 118:3049–3059.

Wasiak, S., R. Zunino, and H.M. McBride. 2007. Bax/Bak promote sumoylation of DRP1 and its stable association with mitochondria during apoptotic cell death. *J. Cell Biol.* 177:439–450.

Wells, R.C., L.K. Picton, S.C. Williams, F.J. Tan, and R.B. Hill. 2007. Direct binding of the dynamin-like GTPase, Dnm1, to mitochondrial dynamics protein Fis1 is negatively regulated by the Fis1 N-terminal arm. *J. Biol. Chem.* 282:33769–33775.

Xia, Z., and D.R. Storm. 2005. The role of calmodulin as a signal integrator for synaptic plasticity. *Nat. Rev. Neurosci.* 6:267–276.

Yokokura, H., M.R. Picciotto, A.C. Nairn, and H. Hidaka. 1995. The regulatory region of calcium/calmodulin-dependent protein kinase I contains closely associated autoinhibitory and calmodulin-binding domains. *J. Biol. Chem.* 270:23851–23859.

Yoon, Y., K.R. Pitts, and M.A. McNiven. 2001. Mammalian dynamin-like protein DLP1 tubulates membranes. *Mol. Biol. Cell.* 12:2894–2905.

Yoon, Y., E.W. Krueger, B.J. Oswald, and M.A. McNiven. 2003. The mitochondrial protein hFis1 regulates mitochondrial fission in mammalian cells through an interaction with the dynamin-like protein DLP1. *Mol. Cell. Biol.* 23:5409–5420.

Youle, R.J., and M. Karbowski. 2005. Mitochondrial fission in apoptosis. *Nat. Rev. Mol. Cell Biol.* 6:657–663.

Yu, T., R.J. Fox, L.S. Burwell, and Y. Yoon. 2005. Regulation of mitochondrial fission and apoptosis by the mitochondrial outer membrane protein hFis1. *J. Cell Sci.* 118:4141–4151.

EFFECTS OF DEFEROXAMINE-ACTIVATED HYPOXIA-INDUCIBLE FACTOR-1 ON THE BRAINSTEM AFTER SUBARACHNOID HEMORRHAGE IN RATS

Tomohito Hishikawa, M.D.
Department of Neurological Surgery, Okayama University Graduate School of Medicine and Dentistry, Okayama, Japan

Shigeki Ono, M.D.
Department of Neurological Surgery, Okayama University Graduate School of Medicine and Dentistry, Okayama, Japan

Tomoyuki Ogawa, M.D.
Department of Neurological Surgery, Okayama University Graduate School of Medicine and Dentistry, Okayama, Japan

Koji Tokunaga, M.D.
Department of Neurological Surgery, Okayama University Graduate School of Medicine and Dentistry, Okayama, Japan

Kenji Sugiu, M.D.
Department of Neurological Surgery, Okayama University Graduate School of Medicine and Dentistry, Okayama, Japan

Isao Date, M.D.
Department of Neurological Surgery, Okayama University Graduate School of Medicine and Dentistry, Okayama, Japan

Reprint requests:
Tomohito Hishikawa, M.D., Department of Cerebrovascular Surgery, National Cardiovascular Center, 5-7-1 Fujishiro-dai, Suita City, Osaka, Japan, 565-8565.
Email: thishi@hsp.ncvc.go.jp

Received, November 26, 2006.
Accepted, March 28, 2007.

OBJECTIVE: Hypoxia-inducible factor (HIF)-1 is a transcription factor that regulates the expression of various neuroprotective genes. The goal of this study was to clarify the relationship between HIF-1 expression and subarachnoid hemorrhage (SAH) and to characterize the effects of deferoxamine (DFO)-induced increases in HIF-1 protein levels on the brainstem and the basilar artery (BA) after experimental SAH.

METHODS: Rat single- and double-hemorrhage models (injected on Days 0 and 2) of SAH were used. We assessed the time courses for HIF-1 protein levels in the brainstems and the BA diameters within 10 minutes and 6 hours on Days 1 and 2 in the single-SAH model, and also on Day 7 in the double-SAH model. After induction of double hemorrhage in rats, DFO was injected intraperitoneally. We then evaluated HIF-1 protein expression and brainstem activity, BA diameter, and brainstem blood flow.

RESULTS: After the rats experienced SAH, HIF-1 protein expression was significantly greater at 10 minutes in the single-injection model and at 7 days in the double-injection model than at similar time points in the control group, and these increases correlated with degrees of cerebral vasospasm. DFO injection resulted in significant increases in HIF-1 protein expression and activity in the brainstems of rats with SAH, compared with the rats with SAH that were given placebos, and the rats without SAH in the double-hemorrhage model. Cerebral vasospasm and reduction of brainstem blood flow were significantly attenuated in the rats that were administered DFO.

CONCLUSION: These results show that a DFO-induced increase in HIF-1 protein level and activity exerts significant attenuation of BA vasospasm and reduction of brainstem blood flow in the rat model of SAH. DFO may be a promising agent for treating clinical SAH.

KEY WORDS: Brainstem, Cerebral vasospasm, Deferoxamine, Hypoxia-inducible factor-1, Rats, Subarachnoid hemorrhage

Neurosurgery 62:232–241, 2008 DOI: 10.1227/01.NEU.0000296989.61911.81 www.neurosurgery-online.com

Cerebral vasospasm after ruptured aneurysmal subarachnoid hemorrhage (SAH) is a great indicator of poor prognosis. Some reports indicate that 13.5% of patients with SAH die or are disabled as a result of vasospasm (17). The limited understanding of the pathophysiological mechanisms of vasospasm in the context of SAH has resulted in a lack of targeted therapies for this complication.

Hypoxia-inducible factor (HIF)-1, which is a heterodimer of α and β subunits, is a transcription factor that mediates various processes including oxygen homeostasis (29, 30, 32, 34), development, ischemia, and tumor angiogenesis (29) and regulates more than 40 genes including erythropoietin, vascular endothelial growth factor (VEGF), and glucose transporter-1 (33). Furthermore, HIF-1α is induced in the contexts of cerebral ischemia (4,15) and cerebral hemorrhage (14), where it exerts a neuroprotective effect. However, there have been no reports that demonstrate the role of HIF-1 on the brainstem during the period of cerebral vasospasm caused by SAH.

Deferoxamine (DFO) is an iron chelator that is used clinically for treatment of primary or secondary hemochromatosis, and experimental

studies suggest that DFO may have neuroprotective properties in association with brain ischemia (26) and edema after cerebral hemorrhage (10, 22) and cerebral vasospasm caused by SAH (2, 7, 8, 18, 38). In addition, DFO has a pharmacological ability to stabilize HIF-1α protein (19, 39). Overexpression of HIF-1α by an iron chelator (3, 27) or by hypoxic preconditioning (3, 28) induces tolerance against cerebral ischemia, and thrombin preconditioning attenuates erythrocyte- and iron-induced brain edema via HIF-1α protein accumulation (9).

In this study, we present the relationship between HIF-1 expression in the brainstem and the diameter of the major cerebral arteries of rats after SAH and, and we evaluate the effects of DFO-induced overexpression in HIF-1α protein level and activity on the brainstem and basilar artery (BA) after SAH.

MATERIALS AND METHODS

Experimental Model of Subarachnoid Hemorrhage

All animal experiments were performed according to the guidelines of the Institutional Animal Care and Use Committee of Okayama University. Male Sprague-Dawley rats that weighed 350 to 400 g were allowed free access to food and water. Rats were anesthetized by an intraperitoneal injection of sodium pentobarbital (1 mg/kg) and were allowed to breathe spontaneously. A midline skin incision was made from the middle of the calvarium to the lower cervical spine with rats placed in the prone position, and the atlanto-occipital membrane was exposed. A 26-gauge needle was inserted into the cisterna magna, and 0.3 mL of autologous arterial blood was injected under sterile conditions. After induction of SAH, rats were placed in a head-down position for 30 minutes to accumulate thick clots around the BA. Control animals received the same volume of saline solution instead of autologous blood.

Study Protocol

To evaluate the relationship between HIF-1 expression and both acute transient and delayed chronic cerebral vasospasm, rat single- and double-hemorrhage models of SAH were used for this study (35). Rats were randomly assigned to one of four groups (Group 1, single hemorrhage; Group 2, single saline injection; Group 3, double hemorrhage; and Group 4, double saline injection). After anesthetization on Day 0, all groups received 0.3 mL of either autologous arterial blood or saline. Groups 3 and 4 underwent reanesthetization 2 days later (on Day 2) and were administered a second injection of either blood or saline. Rats in Groups 1 and 2 were decapitated either at 10 minutes (Group 1, n = 29 rats; Group 2, n = 14 rats), 6 hours (Group 1, n = 25 rats; Group 2, n = 11 rats), 24 hours/Day 1 (Group 1, n = 25 rats; Group 2, n = 10 rats), or 48 hours/Day 2 (Group 1, n = 28 rats; Group 2, n = 11 rats) after injection, and rats in Groups 3 and 4 were sacrificed 5 days after the second injection on Day 7 (Group 3, n = 21 rats; Group 4, n = 10 rats). Immediately after the rats were sacrificed, the brainstems were harvested and stored in liquid nitrogen for use in the protein and messenger ribonuclieic acid (mRNA) assays.

Vasospasm was assessed by measurement of the BA lumen area in rats from Groups 1 (10 min, 6 h, Days 1 and 2) and 3 (Day 7) (n = 5 rats per group). Rat tissues were fixed by perfusion of 140 mL of phosphate-buffered saline and subsequent infusion of 140 mL of 4% paraformaldehyde in phosphate-buffered saline at physiological blood pressure. The brains were removed and stored in 4% paraformaldehyde overnight and then soaked in 30% sucrose for 48 hours at 4°C. Frozen sections (10 μm) of the BA and brainstem were cryostatically generated, and BA areas were measured under a light microscope equipped with a micrometer. BA cross sections were evaluated to record measurements at two points, namely, the midpoint between the union of the vertebral arteries and the anterior inferior cerebellar arteries, and the midpoint between the anterior inferior cerebellar arteries and the tip of the BA. The mean of the two points was used as the BA area. The ratio of the BA areas to normal BA areas (before injection) was used to assess the degree of cerebral vasospasm.

Deferoxamine Administration

A rat double-hemorrhage model was used to assess the effects of DFO (Sigma-Aldrich, St. Louis, MO) on the brainstem and BA during delayed vasospasm after SAH. The first injection of autologous arterial blood was performed on Day 0, and the second injection was performed on Day 2. On Day 4, rats were administered 300 mg/kg of DFO intraperitoneally (SAH-DFO group, n = 23 rats). Another set of rats was treated with distilled water (SAH-placebo group, n = 22 rats) and used as controls. Both groups were compared with Group 4 (double saline injection, n = 18 rats) to evaluate HIF-1α mRNA protein expression and activity, VEGF mRNA expression, and brainstem blood flow. BA areas were measured for rats from both the SAH-DFO and SAH-placebo groups (n = 5 rats per group) on Day 7 using the same methods described above, and the effects of DFO on BA were also assessed.

Reverse-Transcriptase Polymerase Chain Reaction

Total mRNA was extracted from the brainstems using TRIzol reagent (Invitrogen Life Technologies, Carlsbad, CA). The mRNA (1 μg) was used for reverse transcription with the SuperScript First-Strand Synthesis System (Invitrogen Life Technologies) in accordance with the manufacturer's recommendations to yield 20 μL of first-strand complementary deoxyribonucleic acid (DNA) solution. HIF-1α and VEGF mRNA levels in the brainstem were assessed via polymerase chain reaction (PCR) using 25 μL of the reverse-transcriptase reaction mixture (Qiagen, Valencia, CA) containing Taq DNA polymerase, 2× Qiagen PCR buffer, 3 mmol/L $MgCl_2$, and 400 μmol/L of each deoxyribonucleotide triphosphate in a final volume of 50 μL. Amplification was performed in a DNA cycler (GeneAmp PCR System 9700; Applied Biosystems, Foster City, CA). Rat HIF-1 oligonucleotide primer sequences were 5'-AAG TCT AGG GAT GCA GCA C-3' and 5'-CAA GAT CAC CAG CAT CTA G-3'. To amplify HIF-1α complementary DNA, samples were kept at 95°C for 5 minutes and then subjected to thermocycling (28 cycles of 30 s at 95°C, 30 s at 53°C, and 1.5 min at 72°C, with a final extension of 5 min at 72°C). Rat VEGF primer sequences were 5'-TGC ACC CAC GAC AGA AGG GGA-3' and 5'-TCA CCG CCT TGG CTT GTC ACA T-3'. Samples were kept at 94°C for 4 minutes and then subjected to thermocycling (26 cycles of 30 s at 94°C, 30 s at 60°C, and 2 min at 72°C, with a final extension of 5 min at 72°C). Rat β-actin primer sequences (internal controls) were 5'-TTG TAA CCA ACT GGG ACG ATA TGG-3' and 5'-GAT CTT GAT CTT CAT GGT GCT AGG-3'. Samples were kept at 94°C for 2 minutes and subjected to thermocycling (22 cycles of 2 min at 94°C, 40 s at 94°C, and 40 s at 60°C, with a final extension of 1 min at 72°C). PCR production was analyzed by electrophoresis on 1.5% agarose gel. Gels were visualized with 0.5% ethidium bromide staining and ultraviolet transillumination. Photographs were obtained with black and white film (Polaroid, Bedfordshire, England). Relative band densities were analyzed with NIH Image 1.61 software (National Institutes of Health, Bethesda, MD).

Western Blot Analysis

For HIF-1α immunoblots, frozen brainstem tissue was homogenized in lysis buffer (1% Nonidet P-40 [Sigma-aldrich], 0.5% sodium deoxycholate, and 0.1% sodium dodecyl sulfate) containing protease inhibitor

cocktail (Complete Mini; Roche Diagnostics, Mannheim, Germany). The protein concentration of the lysates was determined by the DC Protein Assay (Bio-Rad Laboratories, Hercules, CA). A double volume of 4× NuPage LDS sample buffer (Invitrogen Life Technologies) was added and boiled at 95°C for 4 minutes. The brainstem samples (100 μg) at each time point were subjected to electrophoresis in a 7.5% sodium dodecyl sulfate-polyacrylamide gel and transferred electrophoretically to a Hybond-P pure nitrocellulose membrane (Amersham Pharmacia Biotech, Buckinghamshire, England). The membranes were probed at room temperature for 2 hours with a 1-to-500 dilution of the primary antibody (mouse monoclonal anti-human HIF-1α [Novus Biologicals, Littleton, CO]), followed by exposure to a 1-to-10,000 dilution of the secondary antibody (peroxidase-conjugated rabbit anti-mouse antibody; Rockland, Gilbertsville, PA) for 45 minutes. The β-actin was analyzed as an internal control by incubation of the membrane with a 1-to-600 dilution of the primary antibody (goat polyclonal anti-human β-actin; Santa Cruz Biotechnology, Santa Cruz, CA) and subsequent incubation with a 1-to-10,000 dilution of the secondary antibody (peroxidase-conjugated donkey anti-goat antibody; Jackson Immunoresearch Laboratories, West Grove, PA). Signal development was performed using an ECL Plus detection kit (Amersham Biosciences). The relative band densities were analyzed using NIH Image software.

Electrophoretic Mobility Shift Assay

Nuclear extracts were prepared from the rat brainstem after rapid dissection and homogenization using a Nuclear Extraction Kit (Panomics, Redwood City, CA). Nuclear protein concentration was determined using the DC Protein Assay, and 5 μg of nuclear protein was used in each lane for electrophoretic mobility shift assays.

DNA-binding activity of HIF-1 was determined using the electrophoretic mobility shift assay Gel Shift Kits (Panomics) and a labeled transcription-factor probe (a biotin-labeled probe) containing the sense-strand sequence of HIF-1 consensus oligonucleotides (5′-AGCTTGCC-CTACGTGCTGTCTCAGA-3′). Binding buffer, polydeoxy(inosinate-cytidylate), and consensus oligonucleotides (10 ng) were then combined and incubated. A total of 5 μg of nuclear extract was loaded onto a 6% polyacrylamide gel, and electrophoresis in Tris-borate ethylenediamine tetraacetic acid (50 mmol/L Tris buffer, 45 mmol/L boric acid, and 0.5 mmol/L ethylenediamine tetraacetic acid) was performed at 120 V for approximately 50 minutes at 4°C. After electrophoresis, the gel was transferred to a Pall Biodyne B membrane (Pall Gelman Laboratory, Ann Arbor, MI) in an electroblotting device at 300 mA for 30 minutes. The membrane was dried and blocked by incubation at room temperature with blocking buffer for 15 minutes and then probed with a 1-to-1000 dilution of streptavidin-horseradish peroxidase conjugate. The membrane was washed three times at room temperature with wash buffer and was incubated with detection buffer for 5 minutes, then with detection buffer plus a working substrate solution for 5 minutes. The membrane was exposed to Hyperfilm ECL (Amersham Biosciences) film. For the competition assay, double-stranded DNA fragments of unlabeled competitor probes (cold transcriptional factor probe) were used under the same conditions.

Brainstem Blood Flow Measurement

Rats were anesthetized and a midline skin incision of the neck was made with the rat in the supine position. Rat body temperature was maintained at 37°C using a heating pad and rectal temperature monitor. The thyroid gland was removed, and the trachea was cannulated to maintain the airway. Arterial blood partial pressure values for oxygen and carbon dioxide, and pH values were monitored and maintained in the respective physiological ranges with a monitoring device (i-STAT; i-STAT Corporation, East Windsor, NJ) and mechanical ventilation. The longus colli and longus capitis muscles beneath the esophagus were retracted bilaterally, and the exposed clivus was drilled out gently. The BA and the ventral surface of the pons were exposed over the dura mater. Brainstem blood flow was measured using laser Doppler flowmetry at 1.5 mm to the right of the BA (SAH-DFO group, n = 5 rats; SAH-placebo group; n = 5 rats, double saline injection group, n = 5 rats) (24).

Statistical Analysis

All data are presented as means ± standard deviations. Comparisons of mRNA and protein levels, vessel areas, and cerebral blood flow (CBF) rates were performed using analysis of variance for multiple comparisons within and between groups, and subsequent pairwise comparisons were made using Fisher's exact test if significant variance was identified. Paired and unpaired *t* tests were used for comparisons between two measurements. Significant differences were considered present at *P* values less than 0.05.

RESULTS

HIF-1α and Protein and VEGF mRNA Levels in the Brainstem after SAH

Reverse transcriptase PCR revealed that HIF-1α mRNA levels were similar when SAH groups and control groups were compared at each time point in both the single- and double-hemorrhage models of SAH in rats (*Fig. 1*). In the rat single-hemorrhage model of SAH, Western blot analysis revealed that the HIF-1α protein level at 10 minutes was significantly greater in rats with SAH than in control rats ($P < 0.01$; *Fig. 2*). Furthermore, the VEGF mRNA level at 10 minutes in rats with SAH was significantly elevated compared with control rats ($P < 0.01$; *Fig. 3*). In the rat double-hemorrhage model of SAH, HIF-1α protein (*Fig. 2*) and VEGF mRNA (*Fig. 3*) expression in rats with SAH increased with statistical significance compared with control rats on Day 7 ($P < 0.05$, respectively).

Chronological Change in BA Area

In the single-injection model, acute vasospasm was maximal at 10 minutes (0.699 ± 0.109 minutes; $P < 0.01$, analysis of variance) and persisted for 6 hours. Mild vasospasm was present on Day 2. In the double-injection model, vasospasm was delayed, and BA area on Day 7 (0.821 ± 0.0280) was significantly reduced compared with the baseline value for BA area ($P < 0.05$; analysis of variance; *Fig. 4*).

HIF-1α mRNA and Protein and VEGF mRNA Levels in the Brainstem after Administration of DFO in a Rat Double-hemorrhage Model of SAH

There was no significant difference in HIF-1α mRNA levels when we compared the double-saline injection, SAH-DFO, and SAH-placebo groups (*Fig. 5*). However, HIF-1α protein and VEGF mRNA levels on Day 7 were significantly higher in the SAH-DFO group than in the double-saline injection and SAH-placebo groups ($P < 0.05$; *Figs. 6* and *7*).

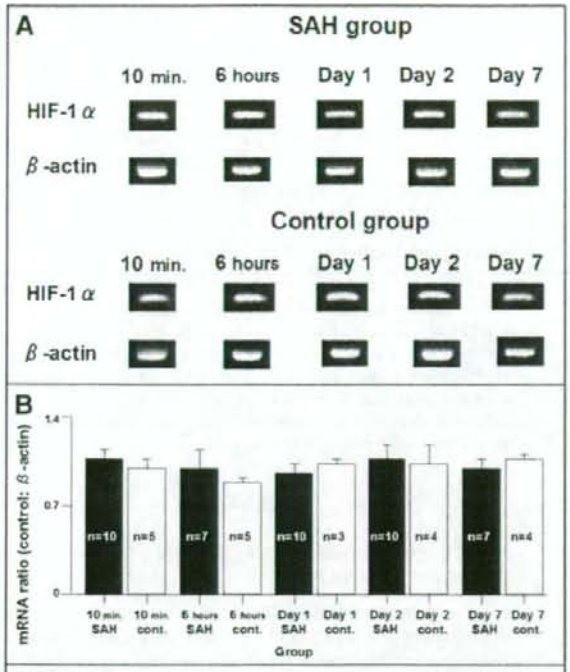

FIGURE 1. A, *representative reverse transcriptase polymerase chain reaction (RT-PCR) amplifications of hypoxia-inducible factor-1α (HIF-1α) and β-actin messenger ribonucleic acid (mRNA) in the rat brainstem at various time points in subarachnoid hemorrhage (SAH)* (top two lanes) *and control groups* (bottom two lanes). B, *semiquantification of RT-PCR bands for each group at each time point. The amount of HIF-1α mRNA is expressed as a ratio of HIF-1α mRNA to β-actin mRNA. There is no significant difference between the SAH groups and the control groups at each time point.*

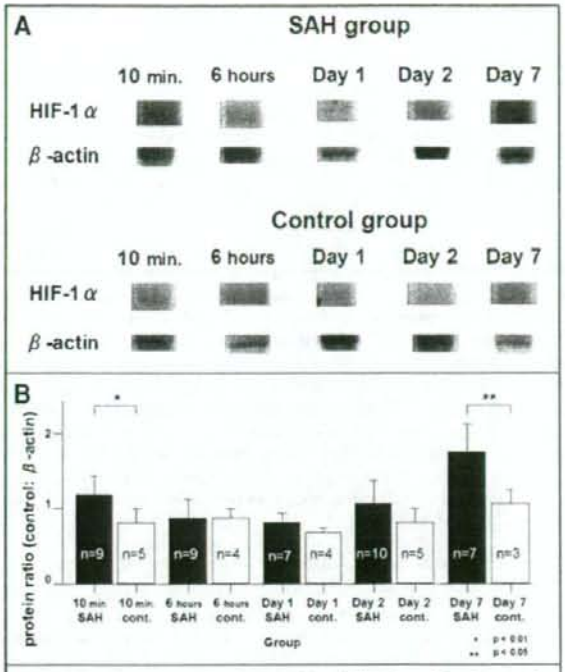

FIGURE 2. A, *representative immunoblots of HIF-1α and β-actin protein from the rat brainstem at various time points in the SAH* (top two lanes) *and control groups* (bottom two lanes). B, *semiquantification of immunoblot bands for each group at each time point. The amount of HIF-1α protein is expressed as a ratio of HIF-1α protein to β-actin protein. The amount of HIF-1α protein at 10 minutes (single-injection model) and 7 days (double-injection model) after SAH is significantly greater than that in the control group* (single asterisk: *10 min, $P < 0.01$*; double asterisk: *Day 7, $P < 0.05$*).

Electrophoretic Mobility Shift Assay

Electrophoretic mobility shift assay studies demonstrated that brainstem HIF-1α activity was elevated in the SAH-placebo group and even more elevated in the SAH-DFO group when compared with the SAH-placebo group (*Fig. 8*). Furthermore, HIF-1α activity was lower in the double saline-injection group than in all other groups.

Effects of DFO Administration on Vasospasm and Cerebral Blood Flow

Intraperitoneal injection of DFO resulted in significantly diminished cerebral vasospasm after SAH (*Fig. 9*). Physiological parameters were maintained within the normal ranges (*Table 1*). For laser Doppler flowmetry-measured blood flow, the CBF was significantly reduced in the SAH-placebo group (26.3 ± 3.98 mL/100 g/min) when compared with the double saline-injection group (41.7 ± 7.57 mL/100 g/min; $P < 0.01$; *Fig. 10*). The administration of DFO in the SAH-DFO group resulted in a significant increase in CBF (46.3 ± 4.55 mL/100 g/min; $P < 0.01$).

DISCUSSION

Our investigation is the first report to examine the time course of HIF-1 expression after experimental SAH and to evaluate the relationship between HIF-1 expression and cerebral vasospasm. This study demonstrated that 1) brainstem HIF-1α protein levels were significantly elevated during the acute (10 min) and chronic (7 day) phases after SAH when compared with the control groups, 2) HIF-1α mRNA levels were similar in the SAH groups and the control groups, 3) changes in VEGF mRNA level paralleled those of HIF-1α protein levels and were significantly higher at 10 minutes and 7 days after SAH when compared with the control group, 4) intraperitoneal administration of DFO (300 mg/kg) on Day 4 in the SAH-DFO group resulted in increased brainstem VEGF mRNA levels and HIF-1α protein expression and activity on Day 7 when compared with the SAH-placebo group, and 5) DFO administration resulted in attenuation of BA vasospasm and an increase in brainstem blood flow on Day 7.

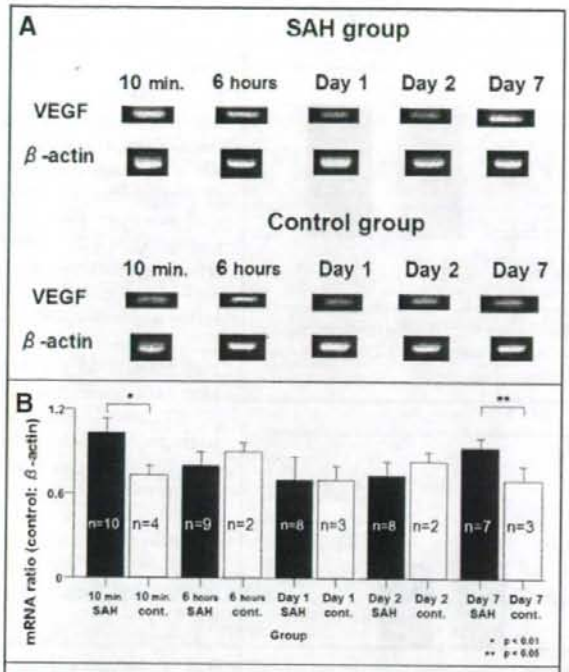

FIGURE 3. A, *representative blots showing RT-PCR amplification of VEGF and β-actin mRNA from the rat brainstem at various time points in the SAH* (top two lanes) *and control groups* (bottom two lanes). B, *semiquantification of RT-PCR bands for each group at each time point. The amount of VEGF mRNA is expressed as a ratio of VEGF mRNA to β-actin mRNA. The amount of VEGF mRNA at 10 minutes and 7 days after SAH is significantly greater than that in the control groups* (single asterisk: *10 min, $P < 0.01$;* double asterisk: *Day 7, $P < 0.05$*).

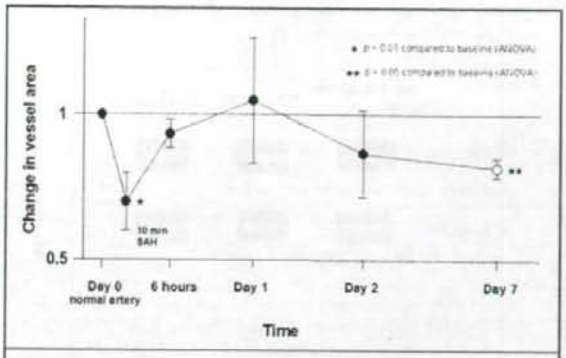

FIGURE 4. *Chronological change of BA area in Groups 1* (filled circles) *and 3* (open circle) *($n = 5$ rats at each time point). Data are expressed as the ratio to baseline (area of normal artery). Significantly different from the baseline values on Day 0 (*$P < 0.01$, **$P < 0.05$ according to analysis of variance [ANOVA]).*

Hypoxia-inducible Factor-1 and Cerebral Vasospasm

HIF-1 is a transcriptional complex that mediates oxygen homeostasis and binds to the HIF-1 DNA binding complex, which is a heterodimer of α and β subunits. In oxygenated cells, the α subunits are unstable and are rapidly destroyed by a mechanism that involves ubiquitination by the von Hippel-Lindau tumor suppressor (pVHL) E3 ligase complex (12). In hypoxic cells, HIF-1α degradation is suppressed, leading to transcriptional activation of target genes. Thus, HIF-1α is essentially regulated not on the mRNA level but on the protein level via protein stabilization.

Several studies have suggested that changes in HIF-1α protein levels may mediate reactive alterations in cellular physiology secondary to cerebral ischemia (4, 15), cerebral hemorrhage (14), and SAH (25). Ostrowski et al. (25) first demonstrated the expression of HIF-1 in brain parenchyma after acute cerebral ischemia in a rat endovascular perforation model of SAH. In the rat single-SAH model used in this study, maximal acute vasospasm occurred at 10 minutes after SAH using a cisternal injection method (5, 35). Jackowski et al. (13) demonstrated that serial measurements of regional CBF (parietal, occipital, and cerebellar cortical regions) by hydrogen clearance revealed that experimental SAH resulted in an immediate 50% global reduction in cortical flow that persisted for up to 3 hours after SAH in rats. Naveri et al. (23) reported that injection of blood immediately decreased CBF, which stabilized after 10 to 15 minutes at approximately 45% of baseline value in a rat single-SAH model. Another investigator (25) described that one of the factors for early brain injury after SAH was acute cerebral ischemia in a rat experimental SAH model. These reports support the idea that the significant elevation of brainstem HIF-1α protein levels during the acute phase after SAH (10 min) is caused by CBF reduction (ischemia) resulting from cerebral vasospasm. In fact, our data show the correlation between the HIF-1α protein expression and the degree of vasoconstriction 10 minutes after SAH. Thrombin can produce brain injury by direct brain cell toxicity, and Jiang et al. (14) reported that thrombin released from a hematoma formed after intracerebral hemorrhage induced an increase in HIF-1α protein content in surrounding brain tissue. Thus, in addition to ischemia, thrombin released from a subarachnoid hematoma could play a role in the increase in HIF-1, which is especially notable for the acute (10 min after SAH) increase in HIF-1. In a rat single-hemorrhage model, late vasoconstriction occurred in 2 days according to Delgado et al. (5). There was mild vasospasm on Day 2 in our study, and a tendency for HIF-1α protein to increase in rats with SAH, but this increase was not significant. One possible explanation is that cortical CBF regained almost normal values by 48 hours after SAH (13), and HIF-1α protein expression was suppressed in some degree because of the recovery of CBF.

A single SAH in rats produced only acute and transient cerebral vasospasm, whereas the double-hemorrhage method of producing SAH in rats resulted in delayed vasospasm that mimicked human vasospasm (20). The present study demonstrated

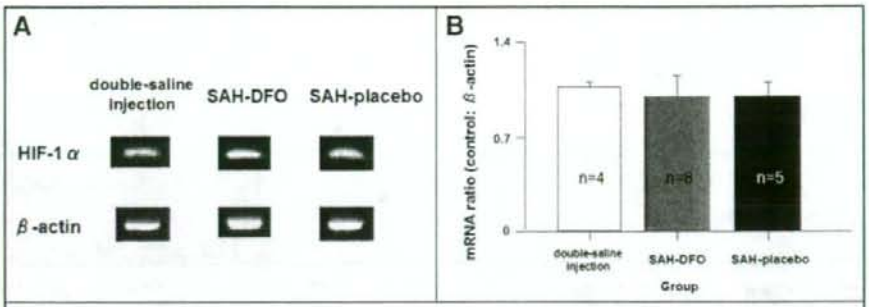

FIGURE 5. A, *representative blots showing RT-PCR amplification of HIF-1α* (top) *and β-actin* (bottom) *mRNA in the double-saline injection, SAH-DFO, and SAH-placebo groups.* B, *semiquantification of RT-PCR bands for each group. There is no significant difference in HIF-1α mRNA levels when comparing all groups.*

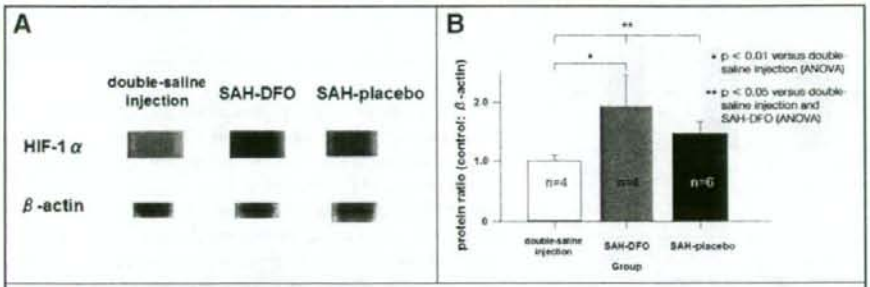

FIGURE 6. A, *representative immunoblots of HIF-1α* (top) *and β-actin* (bottom) *protein in the double-saline injection, SAH-DFO, and SAH-placebo groups.* B, *semiquantification of immunoblot bands for each group. There is a significant increase in HIF-1α protein in the SAH-DFO group when compared with the double-saline injection group ($P < 0.01$, ANOVA) and the SAH-placebo group ($P < 0.05$, ANOVA).*

that brainstem HIF-1α protein levels correlated with vasospasm on Day 7 (delayed vasospasm) in the double-hemorrhage rat models. CBF measurement of the brainstem revealed an approximately 50% reduction 7 days after SAH compared with the saline-injection group. Vatter et al. (37) indicated an enhanced delayed reduction in CBF in the rat double-hemorrhage model. One of the most possible factors leading to an increase in HIF-1α protein and activity levels during the delayed phase after SAH may be vasospasm-induced brainstem ischemia.

The upstream and downstream signal transduction elements after SAH that mediate the increase in HIF-1α and transduce its neuroprotective effects remain unclear. VEGF is one of the genes in control of HIF-1, and it has angiogenetic and neuroprotective effects on central neurons (15). Jin et al. (15) demonstrated that hypoxia-sensitive VEGF signaling could be induced in neurons in global cerebral ischemia via HIF-1 activation. Ostrowski et al. (25) directly proved the close relation between HIF-1α and VEGF protein in the rat brainstem 24 hours after SAH. In our experiment, VEGF mRNA expression was correlated with HIF-1α protein expression at 10 minutes and 7 days after SAH. These data suggest that HIF-1α protein activated VEGF mRNA and that the HIF-1/VEGF pathway existed during the acute and delayed phase after SAH. However, it is unclear how its pathway is related to a response to neuronal damage resulting from SAH in the brainstem, because the neuroprotective effect of VEGF was not directly evaluated in our study.

This experiment also revealed that HIF-1α mRNA was constitutively expressed and was not associated with HIF-1α protein expression. HIF-1α activity was not mediated by altered transcription and was controlled on the protein level in circumstances such as SAH. It is thought that the difference between mRNA and protein expression for HIF-1α is mediated by vasospasm-induced ischemia, which inhibits the ubiquitin-proteosome degradation system (12).

Richard et al. (31) reported that angiotensin II, thrombin, and platelet-derived growth factor could induce an increase in HIF-1α protein levels in vascular smooth muscle cells via reduced nicotinamide adenine dinucleotide phosphate oxidase-mediated reactive oxygen species production under normal oxygen conditions. They concluded that reactive oxygen species upregulated HIF-1 expression by hypoxia-independent (O_2 concentration-independent) mechanisms, and that these mechanisms should play a major role in vascular remodeling (31). Angiotensin II, thrombin, platelet-derived growth factor, and reactive oxygen species are also candidates for spasmogens (1, 21, 36, 42). Thus, changes in HIF-1α protein levels within the vascular wall may also play a role in vasoreactivity after SAH.

Effects of Deferoxamine-activated Hypoxia-inducible Factor-1 on the Brainstem after SAH

To evaluate the effects of DFO on the delayed chronic cerebral vasospasm, a rat double-hemorrhage model of SAH was used in this session of the experiments. DFO is an iron chelator that may protect against brain injury by preventing lipid peroxidation and free radical formation. Indeed, DFO attenuated cerebral vasospasm after experimental SAH (7, 18, 38) and inhibited the production of hydroxyl radicals and progression of brain edema after ischemia in neonatal rats (26). DFO ameliorated brain edema after intracerebral hemorrhage in rats by reducing the oxidative stress caused by the release of iron from

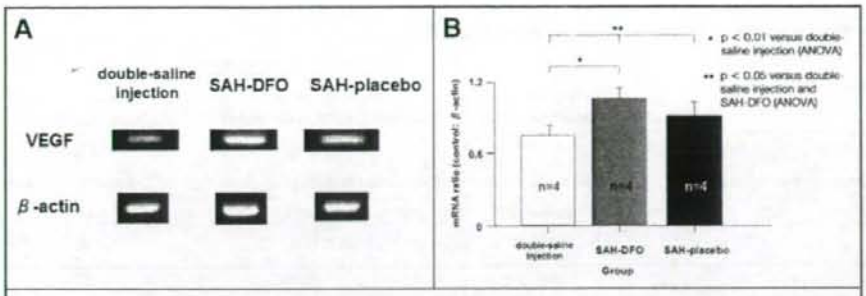

FIGURE 7. A, *representative blots showing RT-PCR amplification of VEGF* (top) *and β-actin* (bottom) *mRNA in the double-saline injection, SAH-DFO, and SAH-placebo groups.* B, *semiquantification of RT-PCR bands for each group. There is significant increase in VEGF mRNA levels in the SAH-DFO group when compared with the double-saline injection group ($P < 0.01$, ANOVA) and the SAH-placebo group ($P < 0.05$, ANOVA).*

extravasated blood (10, 22). DFO is known to stabilize HIF-1α and lead to transcriptional activity of its target genes, as does hypoxia or cobalt chloride (19, 39). Because the association of the von Hippel-Lindau tumor suppressor with HIF-1 is iron dependent, the pVHL/HIF-1 complex cannot form in the cells treated with DFO or cobalt chloride (19). In fact, the interaction between pVHL and HIF-1 is regulated by prolyl hydroxylase, and the requirement of molecular oxygen and iron for prolyl hydroxylase activity may account for the stabilization of HIF-1α observed under hypoxic conditions or after treatment with DFO (11, 12).

Prass et al. (27) recently reported that DFO had neuroprotective effects against focal cerebral ischemia via an increase in the DNA binding of HIF-1α in a middle cerebral artery occlusion model in rats. In this study (27), they proved that intraperitoneal injection of DFO induced tolerance with a maximum effect when given 3 days before ischemia induction at a dose of 300 mg/kg body weight. According to their results, DFO at the same dose was administered intraperitoneally 3 days before Day 7, because cerebral vasospasm is most prominent on Day 7 in a rat double-hemorrhage model of SAH (35). In addition, other studies (3, 9, 28) demonstrated that hypoxia or thrombin preconditioning activates HIF-1α and is neuroprotective against various brain injuries. In our investigation, intraperitoneal administration of DFO in a rat double-hemorrhage model resulted in an increase in brainstem HIF-1α protein levels and caused an improvement in brainstem blood flow and a reduction in cerebral vasospasm.

One possible explanation for the antivasospastic effect of DFO is that DFO itself has the ability to chelate iron. Free iron from a subarachnoid clot catalyzes the generation of cytotoxic free radicals and induces vasospasm (38). Vollmer et al. (38) demonstrated that the iron-chelating agent DFO ameliorated vasospasm in a rabbit model of SAH and that the mechanism of iron chelation suppressed the generation of free radicals. Moreover, iron chelation might also be of direct benefit in reducing neural parenchymal injury induced by free radicals that occurs as a result of ischemia (40). This direct neuroprotec-

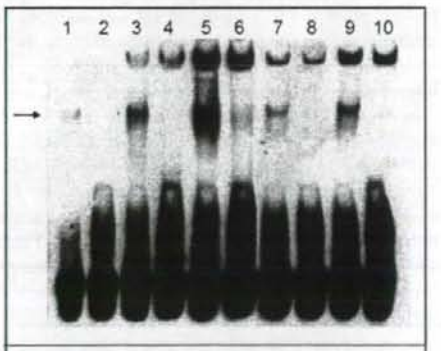

FIGURE 8. *The electrophoretic mobility shift assay for the HIF-1α-binding site. The HIF-1α-specific bands are indicated* (arrow). Lanes 1 *and* 2, *double-saline injection group;* lanes 3 *through* 6, *SAH-DFO group;* lanes 7 *through* 10, *SAH-placebo group.* Lanes 1, 3, 5, 7, *and* 9, *HIF-1α probe and nuclear extracts in each group;* lanes 2, 4, 6, 8, *and* 10, *cold HIF-1α probe (unlabeled competitor) and nuclear extracts in each group.*

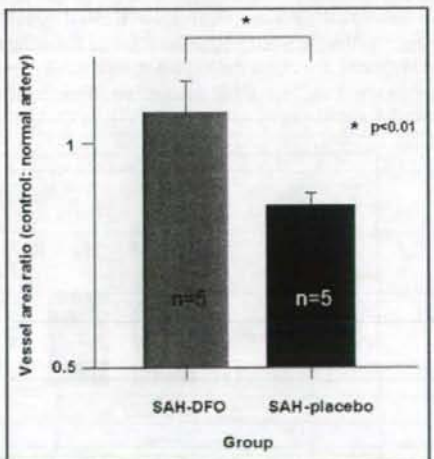

FIGURE 9. *BA area ratio to baseline in the SAH-DFO and SAH-placebo groups ($n = 5$ rats per group). Data show significantly increased area in the SAH-DFO group when compared with the SAH-placebo group, according to the unpaired t test ($P < 0.01$).*

TABLE 1. Physiological variables for effects of deferoxamine on brainstem blood flow[a]

Parameter	Group (n = 5 rats/group)		
	Double-saline injection	Subarachnoid hemorrhage-deferoxamine	Subarachnoid hemorrhage-placebo
Arterial partial pressure of carbon dioxide (mmHg)	45.0 ± 7.2	46.7 ± 4.6	44.0 ± 4.1
Arterial partial pressure of oxygen (mmHg)	69.0 ± 3.2	74.0 ± 9.3	69.5 ± 9.6
pH	7.39 ± 0.056	7.37 ± 0.016	7.42 ± 0.03
Body temperature (°C)	37.2 ± 0.078	37.2 ± 0.60	37.8 ± 0.59

[a] All values are expressed as means ± standard deviations.

tive effect of DFO possibly relates to significant attenuation of the brainstem blood flow reduction that was identified in this experiment.

In our investigation, the change of HIF-1 expression in the vascular wall after DFO administration was not assessed. If DFO induces overexpression of HIF-1 in the vascular wall, it is thought that another possible mechanism for the antivasospastic effect of DFO is HIF-1-induced expression of the genes in its downstream. Grasso et al. (6) reported that systemic administration of human recombinant erythropoietin reduced BA vasoconstriction in a rabbit SAH model and concluded that erythropoietin may exert a direct effect on cerebral arteries via erythropoietin receptors or by acting to induce endothelial release of nitric oxide. Furthermore, Ono et al. (24) reported that overexpression of heme oxygenase-1, the principal enzyme involved in the metabolism of hemoglobin, inhibited arterial contractions induced by hemoglobin and reduced vasospasm after experimental SAH. The expression of these antivasospastic genes, which are activated by HIF-1, may contribute to the significant amelioration of BA vasospasm in a rat SAH model, although the expression of these genes in BA were not evaluated. The DFO administration (in the SAH-DFO groups) significantly elevated VEGF mRNA levels in brainstem compared with the placebo administration (the SAH-placebo groups) in this study. The VEGF expression in cerebral vessels and neurons enhanced angiogenesis during the chronic phase after SAH in rats (16). We may speculate that overexpression of HIF-1-induced VEGF by DFO emphasized angiogenesis in the brainstem and caused improvement in the reduction of brainstem blood flow. Because many investigators have shown the neuroprotective effects of erythropoietin via HIF-1 activation (27, 28, 41), the relationship of other neuroprotective genes in the control of HIF-1 and erythropoietin to the amelioration of reduction of blood flow should be taken into consideration. We hypothesize that the upregulation of HIF-1α protein in the condition of the brain after SAH is a reaction to neuronal damage, and that overexpression of HIF-1α protein by DFO has a neuroprotective effect on the brainstem, in part via DFO itself as an iron chelator, and in part via HIF-1α and the genes that are downstream.

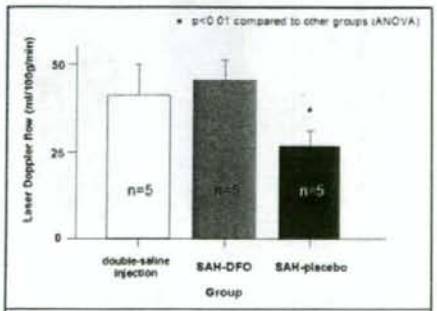

FIGURE 10. *Laser Doppler flowmetry measured blood flow in brainstem in the double-saline injection, SAH-DFO, and SAH-placebo groups. The flow in the SAH-DFO group was significantly higher than that in the SAH-placebo group (*P < 0.0, ANOVA).*

This study suggests that DFO is a promising agent for treating experimental cerebral vasospasm. DFO is clinically used at present, and its safety has been proved. To be convinced of the efficacy of DFO for cerebral vasospasm, we think that additional investigations are needed to clarify the following: 1) Is the effect of DFO via HIF-1 on vasospasm present in large-animal models of SAH such as dogs and primates? 2) How does HIF-1α protein expression change in vascular walls at several time points after experimental SAH? 3) One gene in the control of HIF-1, such as erythropoietin, VEGF, and heme oxygenase-1, should be focused on, and how the gene displays the neuroprotective and antivasospastic effects on the brain after SAH should be explored. 4) DFO brain concentration and its pharmacokinetic parameters after intraperitoneal injection should be evaluated to determine the adequate dosage of DFO.

CONCLUSION

We report that HIF-1α protein expression increased in the brainstem during the acute and delayed phases after SAH, and that a DFO-induced additional increase in HIF-1α protein levels and activity exerted significant attenuation of BA vasospasm and a reduction in brainstem blood flow in the rat model of SAH. DFO has potential as a therapeutic agent for

cerebral vasospasm caused by aneurysmal SAH via upregulation of HIF-1 activity.

REFERENCES

1. Andrews P, Papadakis N, Gavras H: Reversal of experimental acute cerebral vasospasm by angiotensin converting enzyme inhibition. **Stroke** 13:480–483, 1982.
2. Arthur AS, Fergus AH, Lanzino G, Mathys J, Kassell NF, Lee KS: Systemic administration of the iron chelator deferiprone attenuates subarachnoid hemorrhage-induced cerebral vasospasm in the rabbit. **Neurosurgery** 41:1385–1392, 1997.
3. Bergeron M, Gidday JM, Yu AY, Semenza GL, Ferriero DM, Sharp FR: Role of hypoxia-inducible factor-1 in hypoxia-induced ischemic tolerance in neonatal rat brain. **Ann Neurol** 48:285–296, 2000.
4. Chavez JC, LaManna JC: Activation of hypoxia-inducible factor-1 in the rat cerebral cortex after transient global ischemia: Potential role of insulin-like growth factor-1. **J Neurosci** 22:8922–8931, 2002.
5. Delgado TJ, Brismar J, Svendgaard NA: Subarachnoid hemorrhage in the rats: Angiography and fluorescence microscopy of the major cerebral arteries. **Stroke** 16:595–602, 1985.
6. Grasso G, Buemi M, Alafaci C, Sfacteria A, Passalacqua M, Sturiale A, Calapai G, De Vico G, Piedimonte G, Salpietro FM, Tomasello F: Beneficial effects of systemic administration of recombinant human erythropoietin in rabbits subjected to subarachnoid hemorrhage. **Proc Natl Acad Sci U S A** 99:5627–5631, 2002.
7. Harada T, Mayberg MR: Inhibition of delayed arterial narrowing by the iron-chelating agent deferoxamine. **J Neurosurg** 77:763–767, 1992.
8. Horky LL, Pluta RM, Boock RJ, Oldfield EH: Role of ferrous iron chelator 2,2'-dipyridyl in preventing delayed vasospasm in a primate model of subarachnoid hemorrhage. **J Neurosurg** 88:298–303, 1998.
9. Hua Y, Keep RF, Hoff JT, Xi G: Thrombin preconditioning attenuates brain edema induced by erythrocytes and iron. **J Cereb Blood Flow Metab** 23:1448–1454, 2003.
10. Huang FP, Xi G, Keep RF, Hua Y, Nemoianu A, Hoff JT: Brain edema after experimental intracerebral hemorrhage: Role of hemoglobin degradation products. **J Neurosurg** 96:287–293, 2002.
11. Ivan M, Kondo K, Yang H, Kim W, Valiando J, Ohh M, Salic A, Asara JM, Lane WS, Kaelin WG Jr: HIFα targeted for VHL-mediated destruction by proline hydroxylation: Implication for O_2 sensing. **Science** 292:464–468, 2001.
12. Jaakkola P, Mole DR, Tian YM, Wilson MI, Gielbert J, Gaskell SJ, Kriegsheim Av, Hebestreit HF, Mukherji M, Schofield CJ, Maxwell PH, Pugh CW, Ratcliffe PJ: Targeting of HIF-1α to the von Hippel-Lindau ubiquitylation complex by O_2-regulated prolyl hydroxylation. **Science** 292:468–472, 2001.
13. Jackowski A, Crockard A, Burnstock G, Russell RR, Kristek F: The time course of intracranial pathophysiological changes following experimental subarachnoid haemorrhage in the rat. **J Cereb Blood Flow Metab** 10:835–849, 1990.
14. Jiang Y, Wu J, Keep RF, Hua Y, Hoff JT, Xi G: Hypoxia-inducible factor-1α accumulation in the brain after experimental intracerebral hemorrhage. **J Cereb Blood Flow Metab** 22:689–696, 2002.
15. Jin KL, Mao XO, Nagayama T, Goldsmith PC, Greenberg DA: Induction of vascular endothelial growth factor and hypoxia-inducible factor-1α by global ischemia in rat brain. **Neuroscience** 99:577–585, 2000.
16. Jośko J: Cerebral angiogenesis and expression of VEGF after subarachnoid hemorrhage (SAH) in rats. **Brain Res** 981:58–69, 2003.
17. Kassell NF, Torner JC, Haley EC Jr, Jane JA, Adams HP, Kongable GL: The international cooperative study on the timing of aneurysm surgery. Part 1: Overall management results. **J Neurosurg** 73:18–36, 1990.
18. Luo Z, Harada T, London S, Gajdusek C, Mayberg MR: Antioxidant and iron-chelating agents in cerebral vasospasm. **Neurosurgery** 37:1154–1159, 1995.
19. Maxwell PH, Wiesener MS, Chang GW, Clifford SC, Vaux EC, Cockman ME, Wykoff CC, Pugh CW, Maher ER, Ratcliffe PJ: The tumor suppressor protein VHL targets hypoxia-inducible factors for oxygen-dependent proteolysis. **Nature** 399:271–275, 1999.
20. Meguro T, Clower BR, Carpenter R, Parent AD, Zhang JH: Improved rat model for cerebral vasospasm studies. **Neurol Res** 23:761–766, 2001.
21. Mori T, Nagata K, Town T, Tan J, Matsui T, Asano T: Intracisternal increase of superoxide anion production in a canine subarachnoid hemorrhage model. **Stroke** 32:636–642, 2001.
22. Nakamura T, Keep RF, Hua Y, Schallert T, Hoff JT, Xi G: Deferoxamine-induced attenuation of brain edema and neurological deficits in a rat model of intracerebral hemorrhage. **J Neurosurg** 100:672–678, 2004.
23. Naveri L, Stromberg C, Saavedra JM: Angiotensin IV reverses the acute cerebral blood flow reduction after experimental subarachnoid hemorrhage in the rat. **J Cereb Blood Flow Metab** 14:1096–1099, 1994.
24. Ono S, Komuro T, Macdonald RL: Heme oxygenase-1 gene therapy for prevention of vasospasm in rats. **J Neurosurg** 96:1094–1102, 2002.
25. Ostrowski RP, Colohan AR, Zhang JH: Mechanisms of hyperbaric oxygen-induced neuroprotection in a rat model of subarachnoid hemorrhage. **J Cereb Blood Flow Metab** 25:554–571, 2005.
26. Palmer C, Roberts RL, Bero C: Deferoxamine posttreatment reduces ischemic brain injury in neonatal rats. **Stroke** 25:1039–1045, 1994.
27. Prass K, Ruscher K, Karsch M, Isaev N, Megow D, Priller J, Scharff A, Dirnagl U, Meisel A: Desferrioxamine induces delayed tolerance against cerebral ischemia in vivo and in vitro. **J Cereb Blood Flow Metab** 22:520–525, 2002.
28. Prass K, Scharff A, Ruscher K, Löwl D, Muselmann C, Victorov I, Kapinya K, Dirnagl U, Meisel A: Hypoxia-induced stroke tolerance in the mouse is mediated by erythropoietin. **Stroke** 34:1981–1986, 2003.
29. Pugh CW, Ratcliffe PJ: Regulation of angiogenesis by hypoxia: role of the HIF system. **Nat Med** 9:677–684, 2003.
30. Ramírez-Bergeron DL, Simon MC: Hypoxia-inducible factor and the development of stem cells of the cardiovascular system. **Stem Cells** 19:279–286, 2001.
31. Richard DE, Berra E, Pouyssegur J: Nonhypoxic pathway mediates the induction of hypoxia-inducible factor 1α in vascular smooth muscle cells. **J Biol Chem** 275:26765–26771, 2000.
32. Semenza GL: Hypoxia-inducible factor 1: Control of oxygen homeostasis in health and disease. **Pediatr Res** 49:614–617, 2001.
33. Semenza GL: Signal transduction to hypoxia-inducible factor 1. **Biochem Pharmacol** 64:993–998, 2002.
34. Semenza GL: Surviving ischemia: Adaptive responses mediated by hypoxia-inducible factor 1. **J Clin Invest** 106:809–812, 2000.
35. Suzuki H, Kanamaru K, Tsunoda H, Inada H, Kuroki M, Sun H, Waga S, Tanaka T: Heme oxygenase-1 gene induction as an intrinsic regulation against delayed cerebral vasospasm in rats. **J Clin Invest** 104:59–66, 1999.
36. Tsurutani H, Ohkuma H, Suzuki S: Effects of thrombin inhibitor on thrombin-related signal transduction and cerebral vasospasm in the rabbit subarachnoid hemorrhage model. **Stroke** 34:1497–1500, 2003.
37. Vatter H, Weidauer S, Konczalla J, Dettmann E, Zimmermann M, Raabe A, Preibisch C, Zanella FE, Seifert V: Time course in the development of cerebral vasospasm after experimental subarachnoid hemorrhage: Clinical and neuroradiological assessment of the rat double hemorrhage model. **Neurosurgery** 58:1190–1197, 2006.
38. Vollmer DG, Hongo K, Ogawa H, Tsukahara T, Kassell NF: A study of the effectiveness of the iron-chelating agent deferoxamine as vasospasm prophylaxis in a rabbit model of subarachnoid hemorrhage. **Neurosurgery** 28:27–32, 1991.
39. Wang GL, Semenza GL: Desferrioxamine induces erythropoietin gene expression and hypoxia-inducible factor 1 DNA-binding activity: Implications for models of hypoxia signal transduction. **Blood** 82:3610–3615, 1993.
40. White BC, Krause GS, Aust SD, Eyster GE: Postischemic tissue injury by iron-mediated free radical lipid peroxidation. **Ann Emerg Med** 14:804–809, 1985.
41. Zaman K, Ryu H, Hall D, O'Donovan K, Lin KI, Miller MP, Marquis JC, Baraban JM, Semenza GL, Ratan RR: Protection from oxidative stress-induced apoptosis in cortical neuronal cultures by iron chelators is associated with enhanced DNA binding of hypoxia-inducible factor-1 and ATF-1/CREB and increased expression of glycolytic enzymes, $p21^{waf1/cip1}$, and erythropoietin. **J Neurosci** 19:9821–9830, 1999.
42. Zhang Z, Nagata I, Kikuchi H, Xue JH, Sakai N, Sakai H, Yanamoto H: Broad-spectrum and selective serine protease inhibitors prevent expression of platelet-derived growth factor-BB and cerebral vasospasm after subarachnoid hemorrhage: Vasospasm caused by cisternal injection of recombinant platelet-derived growth factor-BB. **Stroke** 32:1665–1672, 2001.

Acknowledgments

We thank Hideki Wakimoto, Masako Arao, and Mayumi Konishi for technical assistance.